Modal based goal-oriented error assessment for timeline-dependent quantities in transient dynamics*

F. Verdugo[1], N. Parés[1,2] and P. Díez[1,3]

[1]Laboratori de Càlcul Numèric (LaCàN),
Universitat Politècnica de Catalunya (UPC),
Jordi Girona 1-3 E-08034 Barcelona, Spain.
[2] Laboratori de Càlcul Numèric (LaCàN),
Escola Universitària d'Enginyeria Tècnica Industrial de Barcelona (EUETIB),
Compte d'Urgell, 187, E-08036, Barcelona, Spain.
[3]Centre Internacional de Mètodes Numèrics en Enginyeria (CIMNE),
Gran Capitán s/n, E-08034 Barcelona, Spain.
Email: {francesc.verdugo,nuria.pares,pedro.diez}@upc.edu

Abstract

This article presents a new approach to assess the error in specific quantities of interest in the framework of linear elastodynamics. In particular, a new type of quantities of interest (referred as timeline-dependent quantities) is proposed. These quantities are scalar time-dependent outputs of the transient solution which are better suited to time-dependent problems than the standard scalar ones, frozen in time. The proposed methodology furnishes error estimates for both the standard scalar and the new timeline-dependent quantities of interest. The key ingredient is the modal-based approximation of the associated adjoint problems which allows efficiently computing and storing the adjoint solution.

The approximated adjoint solution is readily post-processed to produce an enhanced solution, requiring only one spatial post-process for each vibration mode and using the time-harmonic hypothesis to recover the time dependence. Thus the proposed goal-oriented error estimate consists in injecting this enhanced adjoint solution into the residual of the direct problem. The resulting estimate is very well suited for transient dynamic simulations because the enhanced adjoint solution is computed before starting the forward time integration of the direct problem. Thus, the cost of the error estimate at each time step is very low.

Keywords: goal-oriented error assessment, elastodynamics, transient dynamics, adjoint problem, quantity of interest, timeline-dependent quantity of interest, modal analysis

1 Introduction

Assessing the reliability and/or improving efficiency of the finite element based approximations has motivated the development of a huge variety of error assessment techniques [1, 2, 3, 4, 5]. The pioneering references on this topic focus in steady-state elliptic problems, e.g. linear elasticity or steady heat transfer. In the context of elliptic problems, the early works consider

*Accepted for publication in the *International Journal for Numerical Methods in Engineering*, May, 9-th 2013.

the energy norm as an error measure [6, 7, 8]. Much later, functionals outputs or *quantities of interest* are introduced to assess the error [9, 10, 11, 12]. The estimates assessing the error in quantities of interest are usually referred in the literature as *goal-oriented* [12]. These techniques are extended to deal with other linear and non-linear problems, as well as to time-dependent problems. The following references illustrate the high variety of applications of the goal-oriented approach: for quasi-steady-state non-linear problems [13, 14, 15, 16], for the advection-diffusion-reaction equation [17], for the stokes problem [18], for parabolic time dependent problems [19, 20, 21] and for coupled problems [22, 23, 24, 25, 26].

Different error estimation techniques are proposed also for second order hyperbolic problems (e.g. wave equation or elastodynamics). In this context, some are providing error indicators to drive mesh adaptive procedures, either using energy-like measures [27, 28, 29, 30, 31, 32] or quantities of interest [33, 34, 35, 36, 37]. Other references introduce error estimates as a quality certification for the numerical approximation, without direct application to adaptivity, see [38, 39, 40] for energy-like error measures and [41, 42, 43, 44, 45, 46, 29] for goal oriented estimates.

To the best knowledge of the authors, the few references cited above as goal oriented error assessment techniques constitute the current state-of-the-art in elastodynamics. This is still an open research topic, with many challenging issues.

The first challenge is reducing the high computational cost of these estimates. Assessing the error in a quantity of interest (instead of the standard energy norm) requires approximating an auxiliary adjoint problem associated with the selected quantity. At the first sight, the numerical computation of this problem is as expensive as the original one. The cost of computing the adjoint problem is reduced using ad-hoc techniques (for instance enriching the adjoint interpolation with handbook functions [41, 42, 44]), but this reduction is not sufficient to make it affordable. Alternative computations of the adjoint solution in time-dependent problems are proposed by [47] using a coarse-scale discretization and [48] using the adjoint solution of an auxiliary steady-state problem.

Moreover, the need of combining the original and adjoint solutions drastically increases the memory requirements. This is because the original solution is solved forwards in time and the adjoint backwards. Thus, in order to combine them, at least one of the two solutions has to be stored in memory as a whole (i.e. for each mesh-degree of freedom and for each time step). Another important overhead is introduced by the post-processing techniques (recovery, equilibration, computation of residuals...) which are required to assess the error. This overhead can be non negligible because the post-processing operations have to be performed at every time step. This extra cost is also present in energy-like estimates but, in the goal oriented context, it can be even higher if the same operations have to be performed for the adjoint problem as well.

Another important issue associated with goal-oriented estimates for elastodynamics (and also for other time-dependent problems) is the definition of the quantity of interest itself. Typically, the quantity is expressed in terms of a (linear) functional, which transforms the solution of the problem into a single representative scalar value. Standard quantities in steady-state problems are averages of the unknown variables in subregions of interest in the computational domain. In time dependent problems the definition of the quantity of interest must involve not only a spatial sub-domain but also a time interval of interest. The choice of this time frame is not always obvious for the end-user. This is because a single scalar value does not provide enough pieces of information about the whole time-space solution. This suggests introducing a new

type of quantities of interest precluding the need of providing the time frame. The output of such a quantity of interest is not anymore a scalar quantity but a time-dependent function. The major novelty of this article is the introduction of this new type of quantities. They are referred as *timeline-dependent* quantities of interest in contrast with the standard *scalar* quantities.

The key ingredient of the proposed methodology is a modal based approximation for the adjoint solution. This is a new approach, with respect to previous goal oriented estimates for elastodynamics [45], which use direct time integration schemes (e.g. Newmark-like methods) to solve the adjoint problem. The modal based strategy is particularly well suited for some particular quantities of interest and allows effectively computing and storing the adjoint problem. Moreover, the use of post-processing techniques in the space domain (flux recovery or equilibration) can be readily applied to the (spatial) description of the modes. Note that this is performed just once for every relevant mode, with no need of carrying out the post-processing at each time step. Dealing with timeline-dependent quantities is much simpler with this approach, because it simplifies the time-translation operation.

The modal-based approach is valid for linear problems and linear quantities of interest. Although a wide range of applications is devised, the modal assessment of the timeline-dependent quantities is valid for some particular cases inducing a time-translation invariance. Moreover, in oder to be competitive with direct time integration methods, a modal approach requires that the quantity of interest is described with a reduced number of vibration modes. These factors could be seen as a limitation of the proposed technique. However, the examples presented here demonstrate that the approach is useful in many practical applications.

The error estimates proposed here are obtained injecting an enhanced adjoint approximation into the weak residual of the original problem. As previously noted, the treatment of the adjoint solution is very efficient, thanks to the modal-based approach. The recovery procedure employed for both eigenvectors and eigenfrequencies is similar to the one proposed by Wiberg *et al.* [49].

The remainder of the paper is structured as follows. Section 2 introduces the equations of elastodynamics, the numerical strategies to solve them and the types of quantities of interest we aim at assessing, in particular the so-called timeline-dependent quantities. Section 3 presents the modal-based error estimate for the standard scalar quantities of interest. Section 4 extends the rationale of previous section to the timeline-dependent quantities. Section 5 contains numerical examples demonstrating the suitability of the proposed estimates. Finally, we draw some concluding remarks.

2 Problem statement

2.1 Governing equations

Consider a visco-elastic body occupying an open bounded domain $\Omega \subset \mathbb{R}^d$, $d \leq 3$, with boundary $\partial\Omega$. The boundary is divided in two disjoint parts, Γ_{N} and Γ_{D} such that $\partial\Omega = \overline{\Gamma}_{\mathrm{N}} \cup \overline{\Gamma}_{\mathrm{D}}$ and the time interval under consideration is $I := [0, T]$. Under the assumption of small perturbations, the evolution of displacements $\mathbf{u}(\mathbf{x}, t)$ and stresses $\boldsymbol{\sigma}(\mathbf{x}, t)$, $\mathbf{x} \in \Omega$ and $t \in I$, is

described by the visco-elastodynamic equations,

$$\rho(\ddot{\mathbf{u}} + a_1\dot{\mathbf{u}}) - \boldsymbol{\nabla}\cdot\boldsymbol{\sigma} = \mathbf{f} \quad \text{in } \Omega\times I, \tag{1a}$$
$$\mathbf{u} = \mathbf{0} \quad \text{on } \Gamma_{\mathrm{D}}\times I, \tag{1b}$$
$$\boldsymbol{\sigma}\cdot\mathbf{n} = \mathbf{g} \quad \text{on } \Gamma_{\mathrm{N}}\times I, \tag{1c}$$
$$\mathbf{u} = \mathbf{u}_0 \quad \text{at } \Omega\times\{0\}, \tag{1d}$$
$$\dot{\mathbf{u}} = \mathbf{v}_0 \quad \text{at } \Omega\times\{0\}. \tag{1e}$$

where an upper dot indicates partial derivation with respect to time, that is $\dot{(\bullet)} := \frac{\mathrm{d}}{\mathrm{d}t}(\bullet)$, and $\mathbf{n}$ denotes the outward unit normal to $\partial\Omega$. The problem data are the mass density $\rho = \rho(\mathbf{x}) > 0$, the first Rayleigh coefficient $a_1 \geq 0$, the body force $\mathbf{f} = \mathbf{f}(\mathbf{x}, t)$ and the traction $\mathbf{g} = \mathbf{g}(\mathbf{x}, t)$ acting on the Neumann boundary $\Gamma_{\mathrm{N}}\times I$. The initial conditions for displacements and velocities are $\mathbf{u}_0 = \mathbf{u}_0(\mathbf{x})$ and $\mathbf{v}_0 = \mathbf{v}_0(\mathbf{x})$ respectively. For the sake of simplicity and without any loss of generality, Dirichlet conditions (1b) are taken as homogeneous.

The set of equations (1) is closed with the constitutive law,

$$\boldsymbol{\sigma} = \boldsymbol{\mathcal{C}} : \boldsymbol{\varepsilon}(\mathbf{u} + a_2\dot{\mathbf{u}}), \tag{2}$$

where the parameter $a_2 \geq 0$ is the second Rayleigh coefficient, $\boldsymbol{\varepsilon}(\mathbf{w}) := \frac{1}{2}(\boldsymbol{\nabla}\mathbf{w} + \boldsymbol{\nabla}^{\mathrm{T}}\mathbf{w})$ is the the kinematic relation (corresponding to small perturbations) and $\boldsymbol{\mathcal{C}}$ is the standard 4th-order elastic Hooke tensor fulfilling

$$\left.\begin{aligned} \boldsymbol{\mathcal{C}}_{ijkl} &= \boldsymbol{\mathcal{C}}_{klij} \quad \text{(major symmetry)},\\ \boldsymbol{\mathcal{C}}_{ijkl} &= \boldsymbol{\mathcal{C}}_{jikl}\\ \boldsymbol{\mathcal{C}}_{ijkl} &= \boldsymbol{\mathcal{C}}_{ijlk} \end{aligned}\right\} \quad \text{(minor symmetries)}.$$

The major symmetry of the stress tensor is used later to derive the constitutive relation of the adjoint problem.

The definition of the weak form of the problem requires introducing the following functional spaces: the standard Sobolev space associated with static displacement fields

$$\boldsymbol{\mathcal{V}}_0 := \left\{\mathbf{w} \in [H^1(\Omega)]^d : \mathbf{w} = \mathbf{0} \text{ on } \Gamma_{\mathrm{D}}\right\},$$

and the Bochner space $\mathcal{L}^2(0, T; \boldsymbol{\mathcal{V}}_0)$ associated with $\boldsymbol{\mathcal{V}}_0$ of square-integrable functions from I into $\boldsymbol{\mathcal{V}}_0$

$$\mathcal{L}^2(0, T; \boldsymbol{\mathcal{V}}_0) := \left\{\mathbf{v} : I \to \boldsymbol{\mathcal{V}}_0, \mathbf{v}(t) \text{ is } \boldsymbol{\mathcal{V}}_0\text{-measurable and } \int_0^T \|\mathbf{v}(t)\|^2_{\boldsymbol{\mathcal{V}}_0} dt < +\infty\right\}.$$

The solution of the problem, $\mathbf{u}(\mathbf{x}, t)$, belongs to the space $\boldsymbol{\mathcal{W}}$ defined as

$$\boldsymbol{\mathcal{W}} := \left\{\mathbf{w} \in \mathcal{L}^2(0, T; \boldsymbol{\mathcal{V}}_0) \text{ with } \dot{\mathbf{w}} \in \mathcal{L}^2(0, T; [\mathcal{L}^2(\Omega)]^d) \text{ and } \ddot{\mathbf{w}} \in \mathcal{L}^2(0, T; \boldsymbol{\mathcal{V}}_0')\right\}$$

and $\boldsymbol{\mathcal{V}}_0'$ denotes the dual space of $\boldsymbol{\mathcal{V}}_0$. Note that in particular this implies that $\mathbf{u} \in \mathcal{C}([0, T]; [\mathcal{L}^2(\Omega)]^d)$ and $\dot{\mathbf{u}} \in \mathcal{C}([0, T]; \boldsymbol{\mathcal{V}}_0')$, see [50]. That is, functions in $\boldsymbol{\mathcal{W}}$ are continuous functions both in space and time, with continuous time derivative.

Remark 1. *Function* $\mathbf{u}$ *is a transformation from* $\Omega \times I$ *and* $\mathbb{R}^d$*, i.e.*

$$\begin{aligned} \mathbf{u} : \Omega \times I &\longrightarrow \mathbb{R}^d \\ (\mathbf{x}, t) &\longmapsto \mathbf{u}(\mathbf{x}, t). \end{aligned}$$

It can also be seen as a transformation from I *and* $\boldsymbol{\mathcal{V}}_0$*, i.e.*

$$\begin{aligned} \mathbf{u} : I &\longrightarrow \boldsymbol{\mathcal{V}}_0 \\ t &\longmapsto \mathbf{u}(t). \end{aligned}$$

In the remainder of the paper, both notations are used, for $\mathbf{u}$ *and other functions, to denote the same mathematical objects depending on the context.*

Thus, the weak form (integrated in space) of problem (1) reads: find $\mathbf{u} \in \boldsymbol{\mathcal{W}}$ veryfing the initial conditions $\mathbf{u}(0) = \mathbf{u}_0$ and $\dot{\mathbf{u}}(0) = \mathbf{v}_0$ and such that for all $t \in I$

$$(\rho(\ddot{\mathbf{u}}(t) + a_1\dot{\mathbf{u}}(t)), \mathbf{w}) + a(\mathbf{u}(t) + a_2\dot{\mathbf{u}}(t), \mathbf{w}) = l(t; \mathbf{w}) \quad \forall \mathbf{w} \in \boldsymbol{\mathcal{V}}_0, \tag{3}$$

where the standard linear and bilinear forms have been introduced

$$a(\mathbf{v}, \mathbf{w}) := \int_\Omega \boldsymbol{\varepsilon}(\mathbf{v}) : \boldsymbol{\mathcal{C}} : \boldsymbol{\varepsilon}(\mathbf{w}) \, \mathrm{d}\Omega \quad , \quad l(t; \mathbf{w}) := (\mathbf{f}(t), \mathbf{w}) + (\mathbf{g}(t), \mathbf{w})_{\Gamma_\mathrm{N}},$$

along with the scalar products

$$(\mathbf{v}, \mathbf{w}) := \int_\Omega \mathbf{v} \cdot \mathbf{w} \, \mathrm{d}\Omega \quad \text{and} \quad (\mathbf{v}, \mathbf{w})_{\Gamma_\mathrm{N}} := \int_{\Gamma_\mathrm{N}} \mathbf{v} \cdot \mathbf{w} \, \mathrm{d}\Gamma.$$

The error estimation strategy presented below, requires a space-time variational framework. The single field formulation introduced by Hughes and Hulbert [51, 52] is considered. Thus, the space-time integrated weak form of (3) reads: find $\mathbf{u} \in \boldsymbol{\mathcal{W}}$ such that

$$B(\mathbf{u}, \mathbf{w}) = L(\mathbf{w}) \quad \forall \mathbf{w} \in \boldsymbol{\mathcal{W}}, \tag{4}$$

where

$$B(\mathbf{v}, \mathbf{w}) := \int_I (\rho(\ddot{\mathbf{v}} + a_1\dot{\mathbf{v}}), \dot{\mathbf{w}}) \, \mathrm{d}t + \int_I a(\mathbf{v} + a_2\dot{\mathbf{v}}, \dot{\mathbf{w}}) \, \mathrm{d}t + (\rho\dot{\mathbf{v}}(0^+), \dot{\mathbf{w}}(0^+)) + a(\mathbf{v}(0^+), \mathbf{w}(0^+))$$

and

$$L(\mathbf{w}) := \int_I l(t; \dot{\mathbf{w}}(t)) \, \mathrm{d}t + (\rho\mathbf{v}_0, \dot{\mathbf{w}}(0^+)) + a(\mathbf{u}_0, \mathbf{w}(0^+)).$$

2.2 Numerical approximation

In the following developments, $\hat{\mathbf{u}} \in \boldsymbol{\mathcal{W}}$ is assumed to be an approximation of the solution of the boundary value problem (1). Note that $\hat{\mathbf{u}}$ must have C^0-continuity in space and C^1-continuity in time. Most typically, the approximation computed with a standard methodology, say $\mathbf{u}^{H,\Delta t}$, does not fulfill these continuity requirements and has to be post-processed to obtain a suitable $\hat{\mathbf{u}}$. Here, $\mathbf{u}^{H,\Delta t}$ is computed using the Newmark method [53], which is widely adopted in practical applications and commercial codes.

A mesh of characteristic element size H discretizing the spatial domain is introduced together with its associated finite element space $\boldsymbol{\mathcal{V}}_0^H \subset \boldsymbol{\mathcal{V}}_0$. The degree of the complete polynomial basis in $\boldsymbol{\mathcal{V}}_0^H$ is denoted by p. This allows introducing the spatially-discrete and time-continuous version of equation (3) (semidiscrete problem), namely: find $\mathbf{u}^H(t) \in \boldsymbol{\mathcal{V}}_0^H$ such that for all $t \in I$

$$(\rho(\ddot{\mathbf{u}}^H(t) + a_1\dot{\mathbf{u}}^H(t)), \mathbf{w}) + a(\mathbf{u}^H(t) + a_2\dot{\mathbf{u}}^H(t), \mathbf{w}) = l(t; \mathbf{w}) \quad \forall \mathbf{w} \in \boldsymbol{\mathcal{V}}_0^H, \tag{5}$$

with initial conditions $\mathbf{u}^H(0) = \boldsymbol{\Pi}^H(\mathbf{u}_0)$ and $\dot{\mathbf{u}}^H(0) = \boldsymbol{\Pi}^H(\mathbf{v}_0)$, being $\boldsymbol{\Pi}^H$ the interpolation operator mapping functions from the continuous space $\boldsymbol{\mathcal{V}}_0$ into the discrete space $\boldsymbol{\mathcal{V}}_0^H$.

The Newmark method is a numerical time-marching scheme providing an approximation of the standard system of second order ODEs (5) arising in structural dynamics. A time-grid discretizing the time interval I is introduced, $\mathcal{T} := \{t_0, t_1, \ldots, t_N\}$, where $0 = t_0 < t_1 < \ldots < t_N = T$. Time steps are denoted by $\Delta t_n := t_n - t_{n-1}$, for $n = 1, \ldots, N$ and the characteristic time step for the time grid is

$$\Delta t := \max_{1 \leq n \leq N} (\Delta t_n).$$

The Newmark solution consists in displacements, velocities and accelerations at each time t_n, $\mathbf{u}_n^{H,\Delta t} \approx \mathbf{u}^H(t_n)$, $\mathbf{v}_n^{H,\Delta t} \approx \dot{\mathbf{u}}^H(t_n)$ and $\mathbf{a}_n^{H,\Delta t} \approx \ddot{\mathbf{u}}^H(t_n)$, for $n = 1, \ldots, N$, such that equation (5) is fulfilled at each time $t_n \in \mathcal{T}$, that is

$$(\rho(\mathbf{a}_n^{H,\Delta t} + a_1\mathbf{v}_n^{H,\Delta t}), \mathbf{w}) + a(\mathbf{u}_n^{H,\Delta t} + a_2\mathbf{v}_n^{H,\Delta t}, \mathbf{w}) = l(t_n; \mathbf{w}) \quad \forall \mathbf{w} \in \boldsymbol{\mathcal{V}}_0^H. \tag{6}$$

Assuming that $\mathbf{u}_{n-1}^{H,\Delta t}, \mathbf{v}_{n-1}^{H,\Delta t}, \mathbf{a}_{n-1}^{H,\Delta t}$ are known and that the following discrete integral expressions hold

$$\mathbf{u}_n^{H,\Delta t} = \mathbf{u}_{n-1}^{H,\Delta t} + \Delta t_n \mathbf{v}_{n-1}^{H,\Delta t} + \frac{1}{2}\Delta t_n^2 \left[(1-2\beta)\mathbf{a}_{n-1}^{H,\Delta t} + 2\beta \mathbf{a}_n^{H,\Delta t}\right],$$
$$\mathbf{v}_n^{H,\Delta t} = \mathbf{v}_{n-1}^{H,\Delta t} + \Delta t_n \left[(1-\gamma)\mathbf{a}_{n-1}^{H,\Delta t} + \gamma \mathbf{a}_n^{H,\Delta t}\right],$$

the only remaining unknown in equation (6) is $\mathbf{a}_n^{H,\Delta t}$, which is obtained solving a linear system of algebraic equations. Similarly, at time t_0, the displacements and velocities are determined by the initial conditions $\mathbf{u}_0$ and $\mathbf{v}_0$ and the acceleration $\mathbf{a}_0^{H,\Delta t}$ is computed by considering that

$$(\rho(\mathbf{a}_0^{H,\Delta t} + a_1\mathbf{v}_0), \mathbf{w}) + a(\mathbf{u}_0 + a_2\mathbf{v}_0, \mathbf{w}) = l_0(\mathbf{w}) \quad \forall \mathbf{w} \in \boldsymbol{\mathcal{V}}_0^H.$$

The scalars β and γ are the parameters of the Newmark method taking values in $[0, 1]$. For $\gamma = 1/2$ the method is second order accurate and there is no numerical damping, whereas for $\gamma > 1/2$ numerical damping is introduced. Moreover, the method is conditionally stable for $\beta \geq \gamma/2 \geq 1/4$. See [53] for specific details.

Note that the Newmark method does not directly provide a numerical approximation $\hat{\mathbf{u}} \in \boldsymbol{\mathcal{W}}$, since the approximation is not even defined in the whole time interval I (it is only given at times t_n of the time grid). The first step in orther to recover the numerical approximation is to extend the Newmark approximation into the whole time domain using a simple piecewise

linear interpolation:

$$\mathbf{u}^{H,\Delta t}(\mathbf{x},t) := \sum_{n=0}^{N} \mathbf{u}_n^{H,\Delta t}(\mathbf{x})\theta_n(t), \tag{7a}$$

$$\mathbf{v}^{H,\Delta t}(\mathbf{x},t) := \sum_{n=0}^{N} \mathbf{v}_n^{H,\Delta t}(\mathbf{x})\theta_n(t), \tag{7b}$$

$$\mathbf{a}^{H,\Delta t}(\mathbf{x},t) := \sum_{n=0}^{N} \mathbf{a}_n^{H,\Delta t}(\mathbf{x})\theta_n(t), \tag{7c}$$

where the functions $\theta_n(t)$, for $n = 0, \dots, N$, are the one-dimensional piecewise linear shape functions related with the time partition $\mathcal{T}$. Note that, however, one cannot take $\hat{\mathbf{u}} = \mathbf{u}^{H,\Delta t}(\mathbf{x},t)$ since this approximation does not meet the regularity requirements of the functional space $\boldsymbol{\mathcal{W}}$; $\mathbf{u}^{H,\Delta t}(\mathbf{x},t) \notin \boldsymbol{\mathcal{W}}$ because its time derivative is not continuous.

Following [2], an admissible approximation $\hat{\mathbf{u}} \in \boldsymbol{\mathcal{W}}$ is easily recovered from the Newmark solution using the information provided by the numerical accelerations, namely

$$\hat{\mathbf{v}}(\mathbf{x},t) := \int_0^t \mathbf{a}^{H,\Delta t}(\mathbf{x},\tau)\ \mathrm{d}\tau + \boldsymbol{\Pi}^H\left(\mathbf{v}_0(\mathbf{x})\right), \tag{8a}$$

$$\hat{\mathbf{u}}(\mathbf{x},t) := \int_0^t \hat{\mathbf{v}}(\mathbf{x},\tau)\ \mathrm{d}\tau + \boldsymbol{\Pi}^H\left(\mathbf{u}_0(\mathbf{x})\right). \tag{8b}$$

Note that by construction the approximation $\hat{\mathbf{u}}$ exactly verifies the initial conditions up to the resolution of the spatial finite element mesh (i.e. $\hat{\mathbf{u}}(0) = \boldsymbol{\Pi}^H(\mathbf{u}_0)$ and $\dot{\hat{\mathbf{u}}}(0) = \boldsymbol{\Pi}^H(\mathbf{v}_0)$) and that the admissible acceleration coincides with the Newmark solution, $\ddot{\hat{\mathbf{u}}} = \mathbf{a}^{H,\Delta t}$. Note that the displacements $\mathbf{u}^{H,\Delta t}$ and $\hat{\mathbf{u}}$ do not coincide but that they both tend to the exact (in time) solution of the semi-discrete problem (5) as Δt tends to zero.

2.3 Scalar and timeline-dependent quantities of interest

A posteriori goal-oriented error estimation techniques aim at assessing the quality of the approximations of scalar outputs of the solution. These techniques are of outmost practical interest because engineering decisions are usually based on representative scalar values of the whole time-space solution $\mathbf{u}$. The scalar output of interest is $s_T := L^{\mathcal{O}}(\mathbf{u})$ and its corresponding approximation is $\hat{s}_T := L^{\mathcal{O}}(\hat{\mathbf{u}})$, where $L^{\mathcal{O}}(\cdot)$ is a bounded linear functional

$$\begin{aligned} L^{\mathcal{O}} : \boldsymbol{\mathcal{W}} &\longrightarrow \mathbb{R} \\ \mathbf{w} &\longmapsto L^{\mathcal{O}}(\mathbf{w}), \end{aligned}$$

extracting a single representative scalar value of the whole time-space solution $\mathbf{u}$. For instance, the quantity of interest can be described as

$$s_T = L^{\mathcal{O}}(\mathbf{u}) := \int_0^T (\mathbf{f}^{\mathcal{O}}(t), \dot{\mathbf{u}}(t))\ \mathrm{d}t + \int_0^T (\mathbf{g}^{\mathcal{O}}(t), \dot{\mathbf{u}}(t))_{\Gamma_{\mathrm{N}}}\ \mathrm{d}t + (\rho\mathbf{v}^{\mathcal{O}}, \dot{\mathbf{u}}(T)) + a(\mathbf{u}^{\mathcal{O}}, \mathbf{u}(T)), \tag{9}$$

where $\mathbf{f}^{\mathcal{O}}$, $\mathbf{g}^{\mathcal{O}}$, $\mathbf{v}^{\mathcal{O}}$ and $\mathbf{u}^{\mathcal{O}}$ are the data characterizing the quantity of interest. The functions $\mathbf{f}^{\mathcal{O}}$ and $\mathbf{g}^{\mathcal{O}}$ extract global or localized averages of velocities in Ω and Γ_{N}, respectively, over the

whole time simulation $[0, T]$ whereas $\mathbf{v}^{\mathcal{O}}$ and $\mathbf{u}^{\mathcal{O}}$ assess averages of velocities and strains or displacements respectively at the final simulation time T.

Goal-oriented error estimation techniques are crucial in assessing the quality of numerical simulations because they provide meaningful information to both drive adaptive mesh refinements or to certify the accuracy of the computations, not only in global measures but also in representative quantities of interest. The extension of standard techniques, developed for static problems, to transient dynamic simulations allows certifying the accuracy of the computations with respect to a single scalar output of the whole space-time solution, but does not provide information of the evolution of the solution during the simulation process. One of the aims of this work is to extend the paradigm of classical goal-oriented error estimation by introducing the new concept of *timeline-dependent quantities of interest*.

Timeline-dependent quantities of interest are defined to be time-dependent functions providing information of the problem variables for all time $t \in [0, T]$. That is, the quantity of interest is no longer a scalar value but a function of time $s(t)$. In contrast with *scalar* quantities of interest which can only be computed having at hand the complete simulation, the timeline-dependent quantity can be produced along the time marching scheme.

To be specific, timeline-dependent quantities of interest are defined as an extension of (9) as

$$s(t) := \int_0^t (\mathbf{f}^{\mathcal{O}}(\tau), \dot{\mathbf{u}}(\tau)) \, \mathrm{d}\tau + \int_0^t (\mathbf{g}^{\mathcal{O}}(\tau), \dot{\mathbf{u}}(\tau))_{\Gamma_{\mathrm{N}}} \, \mathrm{d}\tau + (\rho \mathbf{v}^{\mathcal{O}}, \dot{\mathbf{u}}(t)) + a(\mathbf{u}^{\mathcal{O}}, \mathbf{u}(t)), \tag{10}$$

where the scalar quantity of interest is recovered for the particular case $s_T = s(T)$. Note that, timeline-dependent quantities of interest can be represented via a bounded mapping

$$\begin{aligned} L^{\mathcal{O}}_{\mathrm{TL}} : \boldsymbol{\mathcal{W}} &\longrightarrow \mathcal{L}^2(I) \\ \mathbf{w} &\longmapsto L^{\mathcal{O}}_{\mathrm{TL}}(\mathbf{w}), \end{aligned}$$

where

$$L^{\mathcal{O}}_{\mathrm{TL}}(\mathbf{w})(t) := \int_0^t (\mathbf{f}^{\mathcal{O}}(\tau), \dot{\mathbf{w}}(\tau)) \, \mathrm{d}\tau + \int_0^t (\mathbf{g}^{\mathcal{O}}(\tau), \dot{\mathbf{w}}(\tau))_{\Gamma_{\mathrm{N}}} \, \mathrm{d}\tau + (\rho \mathbf{v}^{\mathcal{O}}, \dot{\mathbf{w}}(t)) + a(\mathbf{u}^{\mathcal{O}}, \mathbf{w}(t)). \tag{11}$$

Thus, the function $L^{\mathcal{O}}_{\mathrm{TL}}(\cdot)$, instead of extracting a scalar value of the whole time-space solution, extracts a function of time, and in particular when applied to the exact solution of the problem $\mathbf{u}$, $L^{\mathcal{O}}_{\mathrm{TL}}(\mathbf{u})(t) = s(t)$ provides a time-dependent function $s \in \mathcal{L}^2(I)$, see figure 1. For the sake of simplicity, the following notation is adopted $L^{\mathcal{O}}_{\mathrm{TL}}(\mathbf{w}; t) := L^{\mathcal{O}}_{\mathrm{TL}}(\mathbf{w})(t)$.

Remark 2. *Note that for a given $t \in I$, the timeline-dependent quantity of interest $s(t)$ defined in* (10) *extracts a scalar value of the time-space solution using information in the time interval $[0, t]$, namely, $s(t) = L^{\mathcal{O}}_{\mathrm{TL}}(\mathbf{u}_{[0,t]})(t)$ and thus can be computed along the time marching scheme. Moreover, the estimates for the quantity of interest $s(t)$ at a given time provide local (in time) error indicators that can be used to adaptively refine the finite element mesh along time.*

The aim of timeline-dependent goal-oriented error estimation strategies is assessing the quality of $\hat{s}(t) = L^{\mathcal{O}}_{\mathrm{TL}}(\hat{\mathbf{u}}; t)$, that is the difference between the exact quantity of interest $s(t) = L^{\mathcal{O}}_{\mathrm{TL}}(\mathbf{u}; t)$ and the approximation obtained with the numerical simulation $\hat{s}(t)$. Note that this has to be estimated for all $t \in I$.

Thus, the goal is to assess and control the error in the quantity of interest which is now a function of time

$$s^{\mathrm{e}}(t) := s(t) - \hat{s}(t).$$

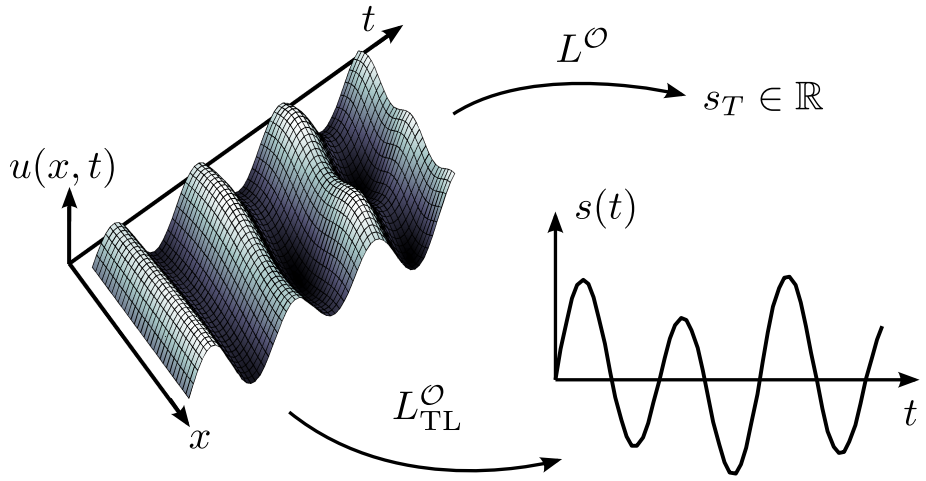

Figure 1: Illustration of scalar and timeline-dependent quantities of interest. The functional $L^{\mathcal{O}}$ maps the time-space solution $\mathbf{u}$ into a scalar value $s_T \in \mathbb{R}$. The operator $L^{\mathcal{O}}_{\mathrm{TL}}$ transforms $\mathbf{u}$ into a time-dependent function $s(t)$.

Recall that the assessment of the error in a scalar quantity, for instance the value of s at $t = T$, $s^e_T := s_T - \hat{s}_T = s(T) - \hat{s}(T) = s^e(T)$, requires introducing an adjoint problem. Thus, s^e_T is estimated in terms of *energy* products of the errors in the direct (or *primal*) and adjoint problems, that have to be integrated both in space and time.

The adjoint problem has the same structure of the direct one, but reverted in time. Consequently, the adjoint solution has to be computed backwards in time and stored beforehand, in order to use it to estimate the error during the forward time-integration of the direct problem. An alternative approach is to solve and store both the direct and the dual problem independently and to compute the error estimate afterwards. However, the latter option does not allow adapting the spatial mesh along the time stepping procedure.

Moreover, the standard numerical integration of the adjoint solution and its storage are often computationally unaffordable. In order to overcome this difficulty, in section 3 the adjoint problem is solved using a modal analysis strategy. This reduces both the computational cost and the memory requirements for the adjoint problem. Moreover, the information provided by modal solution of the adjoint problem is straightforwardly used to adapt the finite element mesh along the computation of the direct problem.

The advantages of using the modal description of the solution of the adjoint problem are even more manifest if dealing with a timeline-dependent quantity of interest, $s(t)$. In this case, there is no longer a single adjoint problem but a family of them, each one associated with each time t in I. For some particular quantities of interest, the members of this family of functions can be generated as a translation in time of a representative member of the family. If this representative member is characterized by a modal description, both the translation and the combination with the solution of the direct problem are simply implemented and computationally efficient. This is described in detail in section 4.

3 A modal-based error representation for scalar quantities of interest

This section is devoted to present a novel approach to assess the error of $\hat{\mathbf{u}}$ measured by a scalar quantity of interest $L^{\mathcal{O}}$ using the modal analysis to obtain a proper approximation of the adjoint solution.

3.1 Error representation and adjoint problem

An auxiliary problem associated with the functional $L^{\mathcal{O}}(\cdot)$, usually denoted by *adjoint* or *dual* problem [29, 46, 41, 42, 43, 44] is introduced to derive an error representation. The variational form of the adjoint problem consists in finding $\mathbf{u}^{\mathrm{d}} \in \boldsymbol{\mathcal{W}}$ such that

$$B(\mathbf{w}, \mathbf{u}^{\mathrm{d}}) = L^{\mathcal{O}}(\mathbf{w}) \quad \forall \mathbf{w} \in \boldsymbol{\mathcal{W}}. \tag{12}$$

The adjoint solution $\mathbf{u}^{\mathrm{d}}$ characterizes the quantity of interest defined by $L^{\mathcal{O}}(\cdot)$. Note that having $\mathbf{u}^{\mathrm{d}}$ at hand allows explicitly computing the quantity of interest associated with the loading described by $L(\cdot)$. This is because if $\mathbf{u}^{\mathrm{d}}$ is available, the quantity $L(\mathbf{u}^{\mathrm{d}})$ is computable and coincides with $L^{\mathcal{O}}(\mathbf{u})$. The associated strong form of the adjoint problem is

$$\rho(\ddot{\mathbf{u}}^{\mathrm{d}} - a_1 \dot{\mathbf{u}}^{\mathrm{d}}) - \boldsymbol{\nabla} \cdot \boldsymbol{\sigma}^{\mathrm{d}} = -\mathbf{f}^{\mathcal{O}} \quad \text{in } \Omega \times I, \tag{13a}$$

$$\mathbf{u}^{\mathrm{d}} = \mathbf{0} \quad \text{on } \Gamma_{\mathrm{D}} \times I, \tag{13b}$$

$$\boldsymbol{\sigma}^{\mathrm{d}} \cdot \mathbf{n} = -\mathbf{g}^{\mathcal{O}} \quad \text{on } \Gamma_{\mathrm{N}} \times I, \tag{13c}$$

$$\mathbf{u}^{\mathrm{d}} = \mathbf{u}^{\mathcal{O}} \quad \text{at } \Omega \times \{T\}, \tag{13d}$$

$$\dot{\mathbf{u}}^{\mathrm{d}} = \mathbf{v}^{\mathcal{O}} \quad \text{at } \Omega \times \{T\}, \tag{13e}$$

with the constitutive law

$$\boldsymbol{\sigma}^{\mathrm{d}} := \boldsymbol{\mathcal{C}} : \boldsymbol{\varepsilon}(\mathbf{u}^{\mathrm{d}} - a_2 \dot{\mathbf{u}}^{\mathrm{d}}). \tag{14}$$

Note that the terms affected by a_1 and a_2 have opposite sign that the ones in the original problem (1). Consequently, the adjoint problem has to be integrated backwards in time, starting from the *final conditions* (13d) and (13e).

The semidiscrete equation associated with the adjoint problem (13) reads: find $\mathbf{u}^{\mathrm{d},H}(t) \in \boldsymbol{\mathcal{V}}_0^H$ verifying the final conditions $\mathbf{u}^{\mathrm{d},H}(T) = \mathbf{u}^{\mathcal{O}}$ and $\dot{\mathbf{u}}^{\mathrm{d},H}(T) = \mathbf{v}^{\mathcal{O}}$ and such that for all $t \in I$

$$(\rho(\ddot{\mathbf{u}}^{\mathrm{d},H}(t) - a_1 \dot{\mathbf{u}}^{\mathrm{d},H}), \mathbf{w}) + a(\mathbf{u}^{\mathrm{d},H}(t) - a_2 \dot{\mathbf{u}}^{\mathrm{d},H}(t), \mathbf{w}) = -l^{\mathcal{O}}(t; \mathbf{w}) \quad \forall \mathbf{w} \in \boldsymbol{\mathcal{V}}_0^H, \tag{15}$$

where $l^{\mathcal{O}}(t; \mathbf{w}) := (\mathbf{f}^{\mathcal{O}}(t), \mathbf{w}) + (\mathbf{g}^{\mathcal{O}}(t), \mathbf{w})_{\Gamma_{\mathrm{N}}}$.

The solution of the adjoint problem $\mathbf{u}^{\mathrm{d}}$ allows representing the error in the quantity of interest in terms of residuals. Indeed, taking $\mathbf{w} = \hat{\mathbf{e}} := \mathbf{u} - \hat{\mathbf{u}}$ in equation (12) yields

$$L^{\mathcal{O}}(\hat{\mathbf{e}}) = B(\hat{\mathbf{e}}, \mathbf{u}^{\mathrm{d}}). \tag{16}$$

The residual error equation for $\hat{\mathbf{e}}$ is readily derived from (4) as

$$B(\hat{\mathbf{e}}, \mathbf{w}) = \hat{R}(\mathbf{w}) := L(\mathbf{w}) - B(\hat{\mathbf{u}}, \mathbf{w}), \text{ for all } \mathbf{w} \in \boldsymbol{\mathcal{W}}, \tag{17}$$

being $\hat{R}(\cdot)$ the weak residual associated with the approximation $\hat{\mathbf{u}}$. Hence, the resulting error representation

$$L^{\mathcal{O}}(\hat{\mathbf{e}}) = \hat{R}(\mathbf{u}^{\mathrm{d}}) \tag{18}$$

allows obtaining the error in the quantity of interest provided that the exact solution of the adjoint problem is available.

Conversely, if an accurate approximation of the adjoint solution is available, say $\tilde{\mathbf{u}}^{\mathrm{d}}$, the error in the quantity of interest is estimated as [21, 46]

$$s_T^e = L^{\mathcal{O}}(\hat{\mathbf{e}}) \approx \hat{R}(\tilde{\mathbf{u}}^{\mathrm{d}}) =: \tilde{s}_T^e. \tag{19}$$

The quality of the functional approximation $\tilde{\mathbf{u}}^{\mathrm{d}}$ is critical to obtain accurate estimates of the error in the scalar quantity of interest.

3.2 Modal-based approximation for the adjoint problem

The *modal analysis* or *mode superposition*, see [54], provides information on the dynamical behavior of the structural system: its natural vibration modes and frequencies. This information is often used to obtain numerical solutions of the problem avoiding the time integration of the complete system of Ordinary Differential Equations resulting from (5). This technique can be used to solve both the primal and adjoint problems, corresponding both to the same structural system (the eigenvalue problem to be solved is the same). Here, this technique is applied to the adjoint problem in order to find a proper approximation $\tilde{\mathbf{u}}^{\mathrm{d}}$.

The natural modes and frequencies of the problem are computed solving the generalized eigenvalue problem associated with the homogeneous undamped version of the semidiscrete problem (either (5) for the primal or (15) for the adjoint). That is, taking $l(t;\mathbf{w}) = 0$ or $l^{\mathcal{O}}(t;\mathbf{w}) = 0$ and $a_1 = a_2 = 0$. Thus, the natural frequencies and modes $(\omega_i^H, \mathbf{q}_i^H) \in \mathbb{R} \times \boldsymbol{\mathcal{V}}_0^H$, $i = 1, \ldots, N_{\mathrm{dof}}$ are the eigenvalues and eigenfunctions of

$$a(\mathbf{q}^H, \mathbf{w}) = (\omega^H)^2(\rho\mathbf{q}^H, \mathbf{w}) \quad \forall \mathbf{w} \in \boldsymbol{\mathcal{V}}_0^H. \tag{20}$$

Note that the number of eigenpairs solution of this problem is the number of degrees of freedom in the computational H-mesh, denoted by N_{dof}. Eigenpairs are sorted from low to high frequencies, namely $\omega_1^H \leq \omega_2^H \cdots \leq \omega_{N_{\mathrm{dof}}}^H$, and eigenvectors are normalized to be orthonormal with respect to the product $(\rho\cdot, \cdot)$, i.e.

$$(\rho\mathbf{q}_i^H, \mathbf{q}_j^H) = \delta_{ij}, \quad 1 \leq i, j \leq N_{\mathrm{dof}}. \tag{21}$$

The modal analysis is applied to obtain the adjoint solution $\mathbf{u}^{\mathrm{d},H}(\mathbf{x}, t)$ by expressing it as a linear combination of the eigenvectors $\mathbf{q}_i^H, i = 1, \ldots, N_{\mathrm{dof}}$, that is

$$\mathbf{u}^{\mathrm{d},H}(\mathbf{x}, t) = \sum_{i=1}^{N_{\mathrm{dof}}} \mathbf{q}_i^H(\mathbf{x}) y_i^H(t). \tag{22}$$

Thus, for the new unknowns of the problem, $y_i^H(t)$, the system of ODEs resulting from (15) is transformed into the uncoupled set of scalar ordinary differential equations

$$\ddot{y}_i^H - [a_1 + a_2(\omega_i^H)^2]\dot{y}_i^H + (\omega_i^H)^2 y_i^H = l_i, \tag{23a}$$

$$y_i^H(T) = u_i, \tag{23b}$$

$$\dot{y}_i^H(T) = v_i, \tag{23c}$$

where the r.h.s. terms l_i, u_i and v_i are computed using the data characterizing the quantity of interest (9) and the eigenvector $\mathbf{q}_i^H$

$$l_i(t) := (\mathbf{f}^{\mathcal{O}}(t), \mathbf{q}_i^H) + (\mathbf{g}^{\mathcal{O}}(t), \mathbf{q}_i^H)_{\Gamma_{\mathrm{N}}},\ u_i := (\rho \mathbf{u}^{\mathcal{O}}, \mathbf{q}_i^H) \text{ and } v_i := (\rho \mathbf{v}^{\mathcal{O}}, \mathbf{q}_i^H). \tag{24}$$

Remark 3. *The time dependent coefficients of the decomposition* (22)*, $y_i^H(t)$, may be computed in many cases by analytically solving* (23)*. In particular, for constant-in-time data $\mathbf{f}^{\mathcal{O}}$ and $\mathbf{g}^{\mathcal{O}}$, the term l_i is also constant in time, and it is easy to see that taking $\alpha = a_1 + a_2 w_i^2$ then*

$$\begin{aligned} y_i^H(t) &= \frac{1}{2} e^{\left(\alpha+\sqrt{\alpha^2-4{\omega_i}^2}\right)(t-T)/2} \left(\frac{2v_i{\omega_i}^2 - \alpha u_i {\omega_i}^2 + \alpha l_i}{{\omega_i}^2\sqrt{\alpha^2-4{\omega_i}^2}} + u_i - \frac{l_i}{{\omega_i}^2} \right) \\ &\quad + \frac{1}{2} e^{\left(\alpha-\sqrt{\alpha^2-4{\omega_i}^2}\right)(t-T)/2} \left(\frac{-2v_i{\omega_i}^2 + \alpha u_i {\omega_i}^2 - \alpha l_i}{{\omega_i}^2\sqrt{\alpha^2-4{\omega_i}^2}} + u_i - \frac{l_i}{{\omega_i}^2} \right) + \frac{l_i}{{\omega_i}^2}, \end{aligned}$$

if $\alpha^2 - 4{\omega_i}^2 \neq 0$. If not, for $\alpha^2 - 4{\omega_i}^2 = 0$

$$y_i^H(t) = \left((u_i - \frac{l_i}{\omega_i^2})(1 + T - t) + (T - t)v_i \right) e^{-\alpha(T-t)/2} + \frac{l_i}{\omega_i^2}.$$

Note that if $\alpha^2 - 4{\omega_i}^2 < 0$, the arguments of the exponential functions are complex numbers but $y_i^H(t)$ remains a real function.

The cost of modal analysis scales as [55, 54, 56]

$$\mathcal{O}(N_{\mathrm{dof}} \cdot N_{\mathrm{bw}}^2) + \mathcal{O}(N_{\mathrm{dof}}^2 \cdot N_{\mathrm{bw}}) + \mathcal{O}(N_{\mathrm{dof}}^3),$$

where N_{bw} denotes the half-bandwidth of the finite element matrices associated with the computational H-mesh. This is computationally unaffordable unless the modal description (22) is truncated up to the first M terms, being $M \ll N_{\mathrm{dof}}$, namely

$$\mathbf{u}^{\mathrm{d},H,M}(\mathbf{x}, t) := \sum_{i=1}^{M} \mathbf{q}_i^H(\mathbf{x}) y_i^H(t). \tag{25}$$

The cost of the truncated modal analysis scales as

$$\mathcal{O}(N_{\mathrm{dof}} \cdot N_{\mathrm{bw}}^2) + \mathcal{O}(N_{\mathrm{dof}} \cdot N_{\mathrm{bw}} \cdot M) + \mathcal{O}(N_{\mathrm{dof}} \cdot M^2).$$

Note that modal analysis is competitive with respect to the Newmark method only if the number of computed eigenvectors M is small when compared with the number of computed time steps N. The cost estimate for the Newmark method reads [54]

$$\mathcal{O}(N_{\mathrm{dof}} \cdot N_{\mathrm{bw}}^2) + \mathcal{O}(N_{\mathrm{dof}} \cdot N_{\mathrm{bw}} \cdot N).$$

Thus, modal analysis is competitive with respect to Newmark method if M is significantly lower than N.

Note that the number of required vibration modes M has to be selected such that the truncated high frequency modes (for $i > M$) are negligible in (22). That is, $\mathbf{u}^{\mathrm{d},H,M}$ is a good approximation to $\mathbf{u}^{\mathrm{d},H}$. This is equivalent to assume that for $i > M$ the values of l_i, u_i and v_i, as defined in (24), are close to zero, and consequently $y_i^H(t) \approx 0$. This is guaranteed if the data $\mathbf{f}^{\mathcal{O}}$, $\mathbf{g}^{\mathcal{O}}$, $\mathbf{u}^{\mathcal{O}}$ and $\mathbf{v}^{\mathcal{O}}$ are well captured by the expansion of the first M eigenvectors.

Remark 4. *The eigenpairs $(\omega_i^H, \mathbf{q}_i^H)$ are H-discrete approximations of the following infinite-dimensional generalized eigenvalue problem: find $\omega \in \mathbb{R}$ and $\mathbf{q} \in \boldsymbol{\mathcal{V}}_0$ such that*

$$a(\mathbf{q}, \mathbf{w}) = \omega^2(\rho\mathbf{q}, \mathbf{w}) \quad \forall \mathbf{w} \in \boldsymbol{\mathcal{V}}_0. \tag{26}$$

The computed eigenfrequencies and eigenvectors $(\omega_i^H, \mathbf{q}_i^H)$, solutions of (20), are good approximations of (26), $(\omega_i, \mathbf{q}_i)$, only for the lower frequency modes [54]. This is supporting the choice of considering only the first M terms in the expansion (22).

3.3 Spatial enhancement of the adjoint approximation

Taking $\tilde{\mathbf{u}}^{\mathrm{d}} = \mathbf{u}^{\mathrm{d},H,M}$ in (19) as an approximation to $\mathbf{u}^{\mathrm{d}}$ provides a raw estimate for the error in the quantity of interest. This requires injecting $\mathbf{u}^{\mathrm{d},H,M}$ as an argument of the residual. However, the resulting value $\hat{R}(\mathbf{u}^{\mathrm{d},H,M})$ is expected to be null if time integration is assumed to be exact or, in any case, very small. This is because $\mathbf{u}^{\mathrm{d},H,M}$ and $\hat{\mathbf{u}}$ have the same spatial resolution, associated with $\boldsymbol{\mathcal{V}}_0^H$, producing an effect analogous to Galerkin orthogonality.

Thus, it is advisory to use an *enhanced* approximation $\tilde{\mathbf{u}}^{\mathrm{d}}$ having a richer space resolution than $\mathbf{u}^{\mathrm{d},H,M}$.

The proposed approach is to find $\tilde{\mathbf{u}}^{\mathrm{d}}$ as a higher order polynomial approximation (piecewise $p+1$ polynomials in the H-mesh), obtained from $\mathbf{u}^{\mathrm{d},H,M}$ using *recovery techniques* [57, 58].

The computed eigenpairs $(\omega_i^H, \mathbf{q}_i^H)$, $i = 1, \ldots, M$ are post-processed into enhanced eigenpairs $(\tilde{\omega}_i, \tilde{\mathbf{q}}_i)$, using a technique similar to [49]. The core of the post-processing technique is computing $\tilde{\mathbf{q}}_i$ from $\mathbf{q}_i^H$ using a space recovery technique described in detail below. Once $\tilde{\mathbf{q}}_i$ is available, $\tilde{\omega}_i$ is readily computed by using Rayleigh coefficients

$$\tilde{\omega}_i := \frac{a(\tilde{\mathbf{q}}_i, \tilde{\mathbf{q}}_i)}{(\rho\tilde{\mathbf{q}}_i, \tilde{\mathbf{q}}_i)}. \tag{27}$$

The enhanced time dependent functions $\tilde{y}_i(t)$ are computed using the enhanced vibration modes $(\tilde{\omega}_i, \tilde{\mathbf{q}}_i)$ solving the set of scalar ODE's

$$\ddot{\tilde{y}}_i - [a_1 + a_2(\tilde{\omega}_i)^2]\dot{\tilde{y}}_i + (\tilde{\omega}_i)^2\tilde{y}_i = \tilde{l}_i, \tag{28a}$$

$$\tilde{y}_i(T) = \tilde{u}_i, \tag{28b}$$

$$\dot{\tilde{y}}_i(T) = \tilde{v}_i, \tag{28c}$$

where $\tilde{l}_i(t) := (\mathbf{f}^{\mathcal{O}}(t), \tilde{\mathbf{q}}_i) + (\mathbf{g}^{\mathcal{O}}(t), \tilde{\mathbf{q}}_i)_{\Gamma_{\mathrm{N}}}$, and $\tilde{u}_i$ and $\tilde{v}_i$ are the coefficients best fitting $\mathbf{u}^{\mathcal{O}}$ and $\mathbf{v}^{\mathcal{O}}$ in the enhanced eigenvector basis, that is

$$\mathbf{u}^{\mathcal{O}} \approx \sum_{i=1}^{N_{\mathrm{dof}}} \tilde{\mathbf{q}}_i(\mathbf{x})\tilde{u}_i \quad \text{and} \quad \mathbf{v}^{\mathcal{O}} \approx \sum_{i=1}^{N_{\mathrm{dof}}} \tilde{\mathbf{q}}_i(\mathbf{x})\tilde{v}_i. \tag{29}$$

Remark 5. *Note that the enhanced eigenvectors $\{\tilde{\mathbf{q}}_i\}_{i=1,\ldots,M}$ are no longer orthonormal. In limit cases, it may even occur that the enhanced eigenvectors are not linearly independent. Thus, the final conditions for the ODE's, $\tilde{u}_i$ and $\tilde{v}_i$, cannot be computed using simple scalar products, like in (24). The values $\tilde{u}_i$ and $\tilde{v}_i$ are computed solving a small least squares problems minimizing the squared error of equations (29). A simpler alternative used in the examples and providing fair results, similar to the least squares approach, is taking $\tilde{u}_i = u_i$ and $\tilde{v}_i = v_i$.*

Finally $\tilde{\mathbf{u}}^{\mathrm{d}}$ is computed as the expansion of enhanced vibration modes, i.e.

$$\tilde{\mathbf{u}}^{\mathrm{d}}(\mathbf{x},t) := \sum_{i=1}^{M} \tilde{\mathbf{q}}_i(\mathbf{x})\tilde{y}_i(t). \tag{30}$$

The recovery procedure for the adjoint solution is performed only once, previous to the direct computation. The harmonic time description is highly efficient because it does not require any further post-process at every time step.

The post-processing technique to enhance the eigenvectors, from $\mathbf{q}_i^H$ to $\tilde{\mathbf{q}}_i$, consists in a local (for each element of the H-mesh) least squares fitting of a $p+1$ degree polynomial.

Let $\Omega_e \subset \Omega$, $e = 1, \ldots, N_{\mathrm{el}}$, be the elements of the H-mesh (N_{el} is the total number of elements). Let $\Omega_e^{\mathrm{patch}}$ denote the patch of elements around Ω_e, consisting of all the elements sharing nodes with Ω_e, and let $\boldsymbol{\mathcal{X}}_e$ and $\boldsymbol{\mathcal{X}}_e^{\mathrm{patch}}$ denote the set of nodes of element Ω_e and patch $\Omega_e^{\mathrm{patch}}$ respectively, see figure 2.

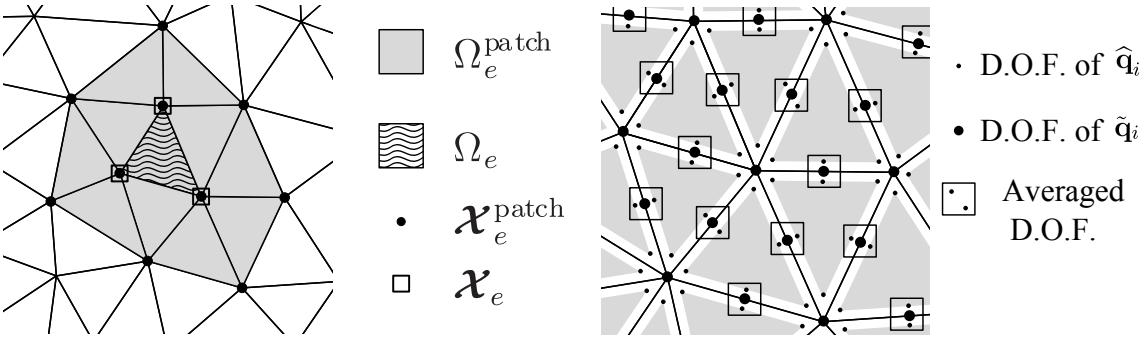

Figure 2: Definition of element patches (left) and illustration of the averaging of discontinuous function $\widehat{\mathbf{q}}_i$ into the continuous function $\tilde{\mathbf{q}}_i$ (right).

The least squares problem stated in each patch $\Omega_e^{\mathrm{patch}}$ reads: find $\mathbf{q}_i^e \in [\mathbb{P}^{p+1}(\Omega_e^{\mathrm{patch}})]^d$ such that $\mathbf{q}_i^e(\mathbf{x}) = \mathbf{q}_i^H(\mathbf{x})$ for $\mathbf{x} \in \boldsymbol{\mathcal{X}}_e$ (it coincides with $\mathbf{q}_i^H$ at the nodes of Ω_e) and

$$\mathbf{q}_i^e = \arg \min_{\mathbf{w} \in [\mathbb{P}^{p+1}(\Omega_e^{\mathrm{patch}})]^d} \sum_{\mathbf{x} \in \boldsymbol{\mathcal{X}}_e^{\mathrm{patch}}} \left(\mathbf{w}(\mathbf{x}) - \mathbf{q}_i^H(\mathbf{x})\right)^2, \tag{31}$$

where $\mathbb{P}^{p+1}(\Omega_e^{\mathrm{patch}})$ denotes the space of polynomials of degree $p+1$ in $\Omega_e^{\mathrm{patch}}$. Problem (31) results in a small linear system of equations for each element of the computational H-mesh.

The post-processed eigenvector $\tilde{\mathbf{q}}_i$ is obtained assembling the contributions of the restriction of the local recovered functions $\mathbf{q}_i^e$ to the corresponding element Ω_e, $\widehat{\mathbf{q}}_i := \sum_e \mathbf{q}_i^e|_{\Omega_e}$. Note that $\widehat{\mathbf{q}}_i$ is discontinuous because, for two neighboring elements Ω_e and $\Omega_{e'}$ with a common side $\Gamma_{ee'} := \bar{\Omega}_e \cap \bar{\Omega}_{e'}$, functions $\mathbf{q}_i^e$ and $\mathbf{q}_i^{e'}$ coincide at the endpoints of $\Gamma_{ee'}$ but, in general, not in the other points of $\Gamma_{ee'}$. In order to build up a continuous approximation $\tilde{\mathbf{q}}_i$, the local contributions are averaged on the element sides. This is simply performed averaging the values of the degrees of freedom associated with the element edges (not vertices), as illustrated in figure 2.

3.4 Practical quantities of interest in modal-based error assessment

The suitability of the modal-based technique introduced above to approximate the solution of the dual problem depends on the particular choice for the quantity of interest. This section presents two types of quantities of interest such that the proposed modal-based estimate is computationally affordable. Note that the cost of building the error estimate is related with the number of eigenmodes M required to properly capture the data characterizing the quantity of interest $\mathbf{f}^{\mathcal{O}}$, $\mathbf{g}^{\mathcal{O}}$, $\mathbf{u}^{\mathcal{O}}$ and $\mathbf{v}^{\mathcal{O}}$. Thus, the quantities of interest presented in this section are selected such that they require a small number of eigenmodes M. Other quantities of interest such as the ones presented in [29, 46, 42, 41, 44] may require a higher number of eigenmodes and, consequently, the proposed technique is not competitive with respect to other alternatives.

The optimal choice to get an efficient response with this approach is selecting a quantity of interest defined using only the first vibration mode

$$L_1^{\mathcal{O}}(\mathbf{u}) := \int_I (\alpha_f \rho \mathbf{q}_1, \dot{\mathbf{u}}(t))\ \mathrm{d}t + (\rho \mathbf{q}_1, \dot{\mathbf{u}}(T)) + a(\alpha_u \mathbf{q}_1, \mathbf{u}(T)). \tag{32}$$

This corresponds to take $\mathbf{f}^{\mathcal{O}} = \alpha_f \rho \mathbf{q}_1$, $\mathbf{g}^{\mathcal{O}} = \mathbf{0}$, $\mathbf{v}^{\mathcal{O}} = \mathbf{q}_1$ and $\mathbf{u}^{\mathcal{O}} = \alpha_u \mathbf{q}_1$ in equation (9). The constants α_f and α_u are introduced in order to obtain consistent dimensions in (32). This quantity has not a direct physical interpretation other than being a sum of averages of velocities (both in time and space and in space for time T) and an energy average of the strains (or stresses) at time T. Moreover, this quantity of interest is computationally inexpensive because requires computing only one vibration mode ($M = 1$).

Note that, following (30), computing the enhanced approximation $\tilde{\mathbf{u}}^{\mathrm{d}}$ associated with (32) and the estimate $\hat{R}(\tilde{\mathbf{u}}^{\mathrm{d}})$ does not require having at hand the exact eigenvector $\mathbf{q}_1$, which is replaced by $\tilde{\mathbf{q}}_1$. Note that this requires taking $\mathbf{f}^{\mathcal{O}} = \alpha_f \rho \tilde{\mathbf{q}}_1$, $\mathbf{g}^{\mathcal{O}} = \mathbf{0}$, $\mathbf{v}^{\mathcal{O}} = \tilde{\mathbf{q}}_1$ and $\mathbf{u}^{\mathcal{O}} = \alpha_u \tilde{\mathbf{q}}_1$ in equations (28) and (29) but not in the definition of the quantity of interest $L_1^{\mathcal{O}}(\mathbf{w})$ in (32). It is worth noting that the numerical experiments (see the example in section 5.2) demonstrate that the estimate $\hat{R}(\tilde{\mathbf{u}}^{\mathrm{d}})$ is a fair approximation of the error measured with the *exact* quantity of interest (taking $\mathbf{q}_1$ and not $\tilde{\mathbf{q}}_1$ in (32)).

A second choice for a suitable quantity is considering the average of displacements at the final time of the computation

$$L_2^{\mathcal{O}}(\mathbf{u}) := (\boldsymbol{\lambda}^{\mathcal{O}}, \mathbf{u}(T)) + (\boldsymbol{\lambda}_{\mathrm{N}}^{\mathcal{O}}, \mathbf{u}(T))_{\Gamma_{\mathrm{N}}}, \tag{33}$$

where the data $\boldsymbol{\lambda}^{\mathcal{O}}$ and $\boldsymbol{\lambda}_{\mathrm{N}}^{\mathcal{O}}$ are weighting functions allowing to localize the average of displacements in some subdomains in Ω and Γ_{N} respectively. The quantity (33) has to be rewritten in the same form as the generic quantity (9) in order to compute its associated enhanced approximation $\tilde{\mathbf{u}}^{\mathrm{d}}$ using the rationale presented above. Thus, the quantity (33) is rewritten as

$$L_2^{\mathcal{O}}(\mathbf{u}) = a(\mathbf{u}^{\mathcal{O}}, \mathbf{u}(T)),$$

taking $\mathbf{f}^{\mathcal{O}} = \mathbf{0}$, $\mathbf{g}^{\mathcal{O}} = \mathbf{0}$, $\mathbf{v}^{\mathcal{O}} = \mathbf{0}$ in equation (9) and being $\mathbf{u}^{\mathcal{O}}$ the solution of the static problem: find $\mathbf{u}^{\mathcal{O}} \in \boldsymbol{\mathcal{V}}_0$ such that

$$a(\mathbf{u}^{\mathcal{O}}, \mathbf{w}) = (\boldsymbol{\lambda}^{\mathcal{O}}, \mathbf{w}) + (\boldsymbol{\lambda}_{\mathrm{N}}^{\mathcal{O}}, \mathbf{w})_{\Gamma_{\mathrm{N}}} \quad \forall \mathbf{w} \in \boldsymbol{\mathcal{V}}_0. \tag{34}$$

Note that here $\mathbf{u}^{\mathcal{O}}$ is not given as part of the data $\boldsymbol{\lambda}^{\mathcal{O}}$ and $\boldsymbol{\lambda}_{\mathrm{N}}^{\mathcal{O}}$ characterizing $L_2^{\mathcal{O}}$. The function $\mathbf{u}^{\mathcal{O}}$ has to be computed as the solution of (34) and therefore $\mathbf{u}^{\mathcal{O}}$ has to be approximated

by some $\tilde{\mathbf{u}}^{\mathcal{O}}$. This enhanced approximation is obtained applying the post-processing technique presented in section 3.3 to the discrete solution $\mathbf{u}^{\mathcal{O},H} \in \boldsymbol{\mathcal{V}}_0^H$ of problem (34). The error estimate $\hat{R}(\tilde{\mathbf{u}}^{\mathrm{d}})$ is readily computed after obtaining an enhanced adjoint approximation $\tilde{\mathbf{u}}^{\mathrm{d}}$, which is obtained using the procedure described in section 3.3 using $\tilde{\mathbf{u}}^{\mathcal{O}}$ instead of $\mathbf{u}^{\mathcal{O}}$. This quantity is more meaningful than the previous one, but it requires in general computing several vibration modes ($M > 1$) in order to properly capture $\tilde{\mathbf{u}}^{\mathcal{O}}$ by the expansion of $\tilde{\mathbf{q}}_i$, $i = 1, \ldots, M$.

4 Assessing timeline-dependent quantities

The first part of this section extends concepts already introduced for scalar quantities, to timeline-dependent quantities. Secondly, an associated error estimate is introduced, based on the modal-based description of the adjoint solution.

4.1 Error representation and family of adjoint problems

Recall that, for a given time $t \in I$, $s(t) = L^{\mathcal{O}}_{\mathrm{TL}}(\mathbf{u}; t)$. In that sense, for this particular value of t, $s(t)$ is seen as a scalar quantity of interest taking t as the *final* time. This scalar quantity of interest is characterized as $L^{\mathcal{O}}(\cdot) = L^{\mathcal{O}}_{\mathrm{TL}}(\cdot; t)$. The associated adjoint problem is analogous to the one presented in 3.1 and reads: find $\mathbf{u}^{\mathrm{d}}_t \in \boldsymbol{\mathcal{W}}|_{[0,t]}$ such that

$$B_t(\mathbf{w}, \mathbf{u}^{\mathrm{d}}_t) = L^{\mathcal{O}}_{\mathrm{TL}}(\mathbf{w}; t) \quad \forall \mathbf{w} \in \boldsymbol{\mathcal{W}}|_{[0,t]}. \tag{35}$$

Note that the solution of this problem is denoted by $\mathbf{u}^{\mathrm{d}}_t$ emphasizing that there is a different solution for each time t. Consequently, equation (35) describes a family of problems, one for each time t. The bilinear form in (35) is defined as

$$\begin{aligned} B_t(\mathbf{v}, \mathbf{w}) := &\int_0^t (\rho(\ddot{\mathbf{v}}(\tau) + a_1 \dot{\mathbf{v}}(\tau)), \dot{\mathbf{w}}(\tau))\ \mathrm{d}\tau + \int_0^t a(\mathbf{v}(\tau) + a_2 \dot{\mathbf{v}}(\tau), \dot{\mathbf{w}}(\tau))\ \mathrm{d}\tau \\ &+ (\rho \dot{\mathbf{v}}(0^+), \dot{\mathbf{w}}(0^+)) + a(\mathbf{v}(0^+), \mathbf{w}(0^+)), \end{aligned}$$

and the space $\boldsymbol{\mathcal{W}}|_{[0,t]}$ denotes the restriction of $\boldsymbol{\mathcal{W}}$ to the time interval $[0, t]$. Analogously as for the derivation of (13), the associated strong form of problem (35) is readily derived as

$$\rho(\ddot{\mathbf{u}}^{\mathrm{d}}_t - a_1 \dot{\mathbf{u}}^{\mathrm{d}}_t) - \boldsymbol{\nabla} \cdot \boldsymbol{\sigma}^{\mathrm{d}}_t = -\mathbf{f}^{\mathcal{O}} \quad \text{in } \Omega \times [0, t], \tag{36a}$$

$$\mathbf{u}^{\mathrm{d}}_t = \mathbf{0} \quad \text{on } \Gamma_{\mathrm{D}} \times [0, t], \tag{36b}$$

$$\boldsymbol{\sigma}^{\mathrm{d}}_t \cdot \mathbf{n} = -\mathbf{g}^{\mathcal{O}} \quad \text{on } \Gamma_{\mathrm{N}} \times [0, t], \tag{36c}$$

$$\mathbf{u}^{\mathrm{d}}_t = \mathbf{u}^{\mathcal{O}} \quad \text{at } \Omega \times \{t\}, \tag{36d}$$

$$\dot{\mathbf{u}}^{\mathrm{d}}_t = \mathbf{v}^{\mathcal{O}} \quad \text{at } \Omega \times \{t\}, \tag{36e}$$

with the constitutive law

$$\boldsymbol{\sigma}^{\mathrm{d}}_t := \boldsymbol{\mathcal{C}} : \boldsymbol{\varepsilon}(\mathbf{u}^{\mathrm{d}}_t - a_2 \dot{\mathbf{u}}^{\mathrm{d}}_t). \tag{37}$$

Recall that the data $\mathbf{f}^{\mathcal{O}}$, $\mathbf{g}^{\mathcal{O}}$, $\mathbf{u}^{\mathcal{O}}$ and $\mathbf{v}^{\mathcal{O}}$ enters in the definition of $L^{\mathcal{O}}_{\mathrm{TL}}(\cdot; t)$ as indicated in (11). Note that for each time t, problem (36) is of the same type as (13) and therefore has to be integrated backwards in time. Thus, the family of adjoint problems associated with the timeline-dependent quantity $L^{\mathcal{O}}_{\mathrm{TL}}$ is a family of standard problems in elastodynamics.

For a particular instance of time t, the error representation of the timeline-dependent quantity of interest $s^{\mathrm{e}}(t)$ is similar to the standard scalar case but taking the adjoint solution $\mathbf{u}_t^{\mathrm{d}}$ related with the particular value $t \in I$, namely

$$s^{\mathrm{e}}(t) = \hat{R}_t(\mathbf{u}_t^{\mathrm{d}}), \tag{38}$$

where

$$\begin{aligned}
&\hat{R}_t(\mathbf{w}) := L_t(\mathbf{w}; t) - B_t(\hat{\mathbf{u}}, \mathbf{w}) \quad \text{and} \\
&L_t(\mathbf{w}) := \int_0^t l(\tau; \dot{\mathbf{w}}(\tau))\, \mathrm{d}\tau + (\rho \mathbf{v}_0, \dot{\mathbf{w}}(0^+)) + a(\mathbf{u}_0, \mathbf{w}(0^+)).
\end{aligned}$$

Hence, an estimate for $s^{\mathrm{e}}(t)$ is obtained injecting an enhanced adjoint approximation $\tilde{\mathbf{u}}_t^{\mathrm{d}}$ in equation (38)

$$s^{\mathrm{e}}(t) \approx \hat{R}_t(\tilde{\mathbf{u}}_t^{\mathrm{d}}). \tag{39}$$

Obviously, it is not possible in practice to independently compute the infinite solutions $\tilde{\mathbf{u}}_t^{\mathrm{d}}$ (one for each time $t \in I$) and then using them in equation (38) to assess $s^{\mathrm{e}}(t)$. However, taking $\mathbf{f}^{\mathcal{O}}$ and $\mathbf{g}^{\mathcal{O}}$ constant in time (which accounts for a number of interesting cases), the different functions $\mathbf{u}_t^{\mathrm{d}}$ corresponding to different time instances are all equivalent after a time translation. Thus, if $\mathbf{u}_t^{\mathrm{d}}$ is properly computed for a particular value of t, for instance $t = T$, the general functions $\mathbf{u}_t^{\mathrm{d}}$ for $t \neq T$ are easily recovered as a direct post-process of $\mathbf{u}_T^{\mathrm{d}}$. This fundamental result, shown in the following theorem, is the crucial observation that allows the error estimation technique to be brought to fruition.

Theorem 1. *For a given t, let $\mathbf{u}_t^{\mathrm{d}}$ be the solution of the adjoint problem defined by equations* (36)*. Assume that data $\mathbf{f}^{\mathcal{O}}$ and $\mathbf{g}^{\mathcal{O}}$ in* (10) *are constant in time, i.e. $\mathbf{f}^{\mathcal{O}}(\mathbf{x}, t) = \mathbf{f}^{\mathcal{O}}(\mathbf{x})$ and $\mathbf{g}^{\mathcal{O}}(\mathbf{x}, t) = \mathbf{g}^{\mathcal{O}}(\mathbf{x})$.*

Then, $\mathbf{u}_t^{\mathrm{d}}$ is related with the adjoint solution associated with the final time T, $\mathbf{u}_T^{\mathrm{d}}$, via the time translation

$$\mathbf{u}_t^{\mathrm{d}}(\tau) = \mathbf{u}_T^{\mathrm{d}}(\tau + T - t). \tag{40}$$

Proof. Let $\mathbf{u}_t^{\star}(\tau) := \mathbf{u}_T^{\mathrm{d}}(\tau + T - t)$. Then, the proof of the theorem follows at once by showing that the solution $\mathbf{u}_t^{\star}(\tau)$ verifies (36).

Observe that the adjoint solution $\mathbf{u}_T^{\mathrm{d}}$ defined in (13) takes values in all the simulation period $I = [0, T]$. When restricting the time interval I to $[T-t, T]$ for a particular $t \in I$, the restricted solution $\mathbf{u}_T^{\mathrm{d}}(s)$, $s \in [T-t, T]$ verifies that

$$\begin{aligned}
\rho(\ddot{\mathbf{u}}_T^{\mathrm{d}} - a_1 \dot{\mathbf{u}}_T^{\mathrm{d}}) - \boldsymbol{\nabla} \cdot \boldsymbol{\sigma}_T^{\mathrm{d}} &= -\mathbf{f}^{\mathcal{O}} \quad \text{in } \Omega \times [T-t, T], \\
\mathbf{u}_T^{\mathrm{d}} &= \mathbf{0} \quad \text{on } \Gamma_{\mathrm{D}} \times [T-t, T], \\
\boldsymbol{\sigma}_T^{\mathrm{d}} \cdot \mathbf{n} &= -\mathbf{g}^{\mathcal{O}} \quad \text{on } \Gamma_{\mathrm{N}} \times [T-t, T], \\
\mathbf{u}_T^{\mathrm{d}} &= \mathbf{u}^{\mathcal{O}} \quad \text{at } \Omega \times \{T\}, \\
\dot{\mathbf{u}}_T^{\mathrm{d}} &= \mathbf{v}^{\mathcal{O}} \quad \text{at } \Omega \times \{T\},
\end{aligned}$$

along with the constitutive law

$$\boldsymbol{\sigma}_T^{\mathrm{d}} := \boldsymbol{\mathcal{C}} : \boldsymbol{\varepsilon}(\mathbf{u}_T^{\mathrm{d}} - a_2 \dot{\mathbf{u}}_T^{\mathrm{d}}).$$

Applying the translation $s = \tau + T - t$, the restricted solution $\mathbf{u}_T^{\mathrm{d}}(s)$ defined in $[T-t, T]$ transforms into $\mathbf{u}_t^\star(\tau) = \mathbf{u}_T^{\mathrm{d}}(\tau + T - t)$ defined in $[0, t]$ veryfing

$$\rho(\ddot{\mathbf{u}}_t^\star - a_1 \dot{\mathbf{u}}_t^\star) - \boldsymbol{\nabla} \cdot \boldsymbol{\sigma}_t^\star = -\mathbf{f}^{\mathcal{O}}(\tau - T + t) \quad \text{in } \Omega \times [0,t], \tag{41a}$$

$$\mathbf{u}_t^\star = \mathbf{0} \qquad \text{on } \Gamma_{\mathrm{D}} \times [0,t], \tag{41b}$$

$$\boldsymbol{\sigma}_t^\star \cdot \mathbf{n} = -\mathbf{g}^{\mathcal{O}}(\tau - T + t) \quad \text{on } \Gamma_{\mathrm{N}} \times [0,t], \tag{41c}$$

$$\mathbf{u}_t^\star = \mathbf{u}^{\mathcal{O}} \qquad \text{at } \Omega \times \{t\}, \tag{41d}$$

$$\dot{\mathbf{u}}_t^\star = \mathbf{v}^{\mathcal{O}} \qquad \text{at } \Omega \times \{t\}, \tag{41e}$$

with the constitutive law

$$\boldsymbol{\sigma}_t^\star := \boldsymbol{\mathcal{C}} : \boldsymbol{\varepsilon}(\mathbf{u}_t^\star - a_2 \dot{\mathbf{u}}_t^\star).$$

Note that, equations (36) and (41) are identical except for the external loads. Thus the result follows from the assumption that the loads $\mathbf{f}^{\mathcal{O}}$ and $\mathbf{g}^{\mathcal{O}}$ are constant in time. □

Theorem (1) allows to efficiently recover the family of enhanced approximations $\tilde{\mathbf{u}}_t^{\mathrm{d}}$ from the enhanced approximation $\tilde{\mathbf{u}}_T^{\mathrm{d}}$ as

$$\tilde{\mathbf{u}}_t^{\mathrm{d}}(\tau) = \tilde{\mathbf{u}}_T^{\mathrm{d}}(\tau + T - t). \tag{42}$$

Consequently, the approximation $\tilde{\mathbf{u}}_T^{\mathrm{d}}$ is the base for assessing the error both in the scalar and timeline-dependent quantities, providing in the latter case more meaningful information. The translation (42) is done very efficiently by means of the modal description of $\tilde{\mathbf{u}}_T^{\mathrm{d}}$:

$$\tilde{\mathbf{u}}_t^{\mathrm{d}}(\tau) = \sum_{i=1}^{M} \tilde{\mathbf{q}}_i \tilde{y}_i(\tau + T - t). \tag{43}$$

Recall that, functions $\tilde{y}_i$ may be known analytically in many cases and therefore computing the translation $y_i(\tau + T - t)$ is inexpensive in that cases.

4.2 Error estimates for timeline-dependent quantities of interest: algorithmic details

The methodology proposed here aims at assessing the error in the timeline-dependent quantity $s^{\mathrm{e}}(t)$ at the computational times $\mathcal{T} = \{t_0, \ldots, t_N\}$ introduced above. Thus, the resulting estimates are $\tilde{s}_j^{\mathrm{e}} \approx s^{\mathrm{e}}(t_j)$ for $j = 0, \ldots, N$. This option could be generalized without any additional conceptual difficulty to use a different set of points $\tilde{t}_0, \ldots, \tilde{t}_{\tilde{N}}$.

Once the recovered solution of the adjoint problem corresponding to t_j, $\tilde{\mathbf{u}}_{t_j}^{\mathrm{d}}$, is available, the estimate $\tilde{s}_j^{\mathrm{e}}$ is computed following equation (39)

$$\tilde{s}_j^{\mathrm{e}} := \hat{R}_{t_j}(\tilde{\mathbf{u}}_{t_j}^{\mathrm{d}}) \quad \text{for } j = 0, \ldots, N.$$

The previous equation is rewritten using the modal description (43) as

$$\tilde{s}_j^{\mathrm{e}} = \sum_{i=1}^{M} \left[\int_0^{t_j} \hat{r}(\tau; \tilde{\mathbf{q}}_i) \dot{\tilde{y}}_i(\tau + T - t_j) \, \mathrm{d}\tau + \hat{r}_{0,v}(\tilde{\mathbf{q}}_i) \dot{\tilde{y}}_i(T - t_j) + \hat{r}_{0,u}(\tilde{\mathbf{q}}_i) \tilde{y}_i(T - t_j) \right], \tag{44}$$

where

$$\hat{r}(\tau;\tilde{\mathbf{q}}_i) := l(\tau;\tilde{\mathbf{q}}_i) - (\rho(\ddot{\hat{\mathbf{u}}}(\tau) + a_1\dot{\hat{\mathbf{u}}}(\tau)),\tilde{\mathbf{q}}_i) - a(\hat{\mathbf{u}}(\tau) + a_2\dot{\hat{\mathbf{u}}}(\tau),\tilde{\mathbf{q}}_i), \tag{45a}$$

$$\hat{r}_{0,u}(\tilde{\mathbf{q}}_i) := a(\mathbf{u}_0 - \mathbf{\Pi}^H\mathbf{u}_0,\tilde{\mathbf{q}}_i), \tag{45b}$$

$$\hat{r}_{0,v}(\tilde{\mathbf{q}}_i) := (\rho(\mathbf{v}_0 - \mathbf{\Pi}^H\mathbf{v}_0),\tilde{\mathbf{q}}_i). \tag{45c}$$

Expressions (44) and (45) describe the proposed error estimate. Note that the quantities $\hat{r}_{0,u}$ and $\hat{r}_{0,v}$ introduced in (45b) and (45c) are independent of the selected time t_j and also of τ. Thus, these two quantities are computed just once for each mode $\tilde{\mathbf{q}}_i$, independently of the number of sampling points selected, N, and the number of time-integration points used to compute the expression in (44). The quantity $\hat{r}$ in (45a) depends on τ but not on t_j and therefore has to be evaluated once for each mode $\tilde{\mathbf{q}}_i$ and for each integration point of the time-quadrature to integrate the expression (44). This suggests taking the same time-integration points for each sampling time t_j (but using only those previous to t_j). The option adopted here is to a use composed Gauss quadrature based on the Newmark time partition. With this choice, the estimate $\tilde{s}^{\mathrm{e}}_j$ is computed as the sum of contributions of the initial conditions and the time steps

$$\tilde{s}^{\mathrm{e}}_j = \sum_{n=0}^{N} \tilde{s}^{\mathrm{e}}_{j,n} \quad \text{for } j = 0,\dots,N,$$

where $\tilde{s}^{\mathrm{e}}_{j,0}$ is defined as

$$\tilde{s}^{\mathrm{e}}_{j,0} := \sum_{i=1}^{M} \left[\hat{r}_{0,v}(\tilde{\mathbf{q}}_i)\dot{\tilde{y}}_i(T-t_j) + \hat{r}_{0,u}(\tilde{\mathbf{q}}_i)\tilde{y}_i(T-t_j)\right],$$

and $\tilde{s}^{\mathrm{e}}_{j,n}$ is defined for $n \neq 0$ as

$$\tilde{s}^{\mathrm{e}}_{j,n} := \begin{cases} \displaystyle\sum_{i=1}^{M} \int_{t_{n-1}}^{t_n} \hat{r}(\tau;\tilde{\mathbf{q}}_i)\dot{\tilde{y}}_i(\tau+T-t_j)\,\mathrm{d}\tau & \text{if } t_j > t_{n-1}, \\ 0 & \text{otherwise.} \end{cases}$$

The algorithm providing the admissible approximation $\hat{\mathbf{u}}$ and the estimates $\tilde{s}^{\mathrm{e}}_j$, $j = 0,\dots,N$, is detailed in algorithm 1.

5 Numerical examples

This section presents the performance of the error estimates both for the scalar and timeline-dependent quantities of interest in three numerical examples.

All the examples are plane stress problems which are approximated in space using linear ($p = 1$) triangles and in time using the Newmark method with parameters $\beta = 1/4$ and $\gamma = 1/2$. The Newmark method is unconditionally stable for this particular choice of β and γ. Therefore, no stability restrictions have to be imposed to the time step length Δt.

5.1 Example 1

This example illustrates the performance of the proposed error estimates in a 2D wave propagation problem. The problem definition is taken from [45] where it is used to test an error estimate providing error bounds in quantities of interest.

Data: Problem geometry (Ω, Γ_{N}, Γ_{D}), final time (T), material data (E, ν, ρ), loads and initial conditions ($\mathbf{f}$, $\mathbf{g}$, $\mathbf{u}_0$, $\mathbf{v}_0$), computational mesh ($\boldsymbol{\mathcal{V}}_0^H$), time partition ($\mathcal{T}$), data defining the timeline quantity of interest ($\mathbf{f}^{\mathcal{O}}$, $\mathbf{g}^{\mathcal{O}}$, $\mathbf{u}^{\mathcal{O}}$, $\mathbf{v}^{\mathcal{O}}$) and number of vibration modes M.

Result: Admissible solution $\hat{\mathbf{u}}$ and timeline error estimates $\tilde{s}_j^{\mathrm{e}}$, $j = 0, \ldots, N$.

`// Modal analysis`

Compute the eigenpairs $(\omega_i^H, \mathbf{q}_i^H)$ and post-process them into $(\tilde{\omega}_i, \tilde{\mathbf{q}}_i)$, $i = 1, \ldots, M$;

`// Adjoint problem`

Compute the values $\tilde{l}_i, \tilde{u}_i, \tilde{v}_i$ (using $\mathbf{f}^{\mathcal{O}}$, $\mathbf{g}^{\mathcal{O}}$, $\mathbf{u}^{\mathcal{O}}$, $\mathbf{v}^{\mathcal{O}}$ and $\tilde{\mathbf{q}}_i$, $i = 1, \ldots, M$) ;

Compute the time dependent functions $\tilde{y}_i(t)$ (using $\tilde{l}_i, \tilde{u}_i, \tilde{v}_i$ and $\tilde{\omega}_i$, $i = 1, \ldots, M$) ;

`// Initialize computation`

Initialize Newmark solution $\mathbf{u}_0^{H,\Delta t} = \boldsymbol{\Pi}^H \mathbf{u}_0$, $\mathbf{v}_0^{H,\Delta t} = \boldsymbol{\Pi}^H \mathbf{v}_0$;

Initialize admissible solution $\hat{\mathbf{u}}(0) = \mathbf{u}_0^{H,\Delta t}$, $\dot{\hat{\mathbf{u}}}(0) = \mathbf{u}_0^{H,\Delta t}$;

Initialize estimate $\tilde{s}_j^{\mathrm{e}} = \tilde{s}_{j,0}^{\mathrm{e}}$, $j = 0, \ldots, N$;

`// Time stepping`

for $n = 1 \ldots N$ **do**

  `// Compute solution`

  Compute Newmark solution $\mathbf{u}_n^{H,\Delta t}$, $\mathbf{v}_n^{H,\Delta t}$, $\mathbf{a}_n^{H,\Delta t}$;

  Compute the admissible solution $\hat{\mathbf{u}}$ in the time interval $[t_{n-1}, t_n]$;

  `// Error assessment`

  Compute contributions to the estimates $\tilde{s}_j^{\mathrm{e}} = \tilde{s}_j^{\mathrm{e}} + \tilde{s}_{j,n}^{\mathrm{e}}$, $j = n, \ldots, N$ (using the admissible solution $\hat{\mathbf{u}}$ and the modal based description of the adjoint $\tilde{\mathbf{q}}_i$ and $\tilde{y}_i$);

end

Algorithm 1: Algorithm for problem approximation and error assessment.

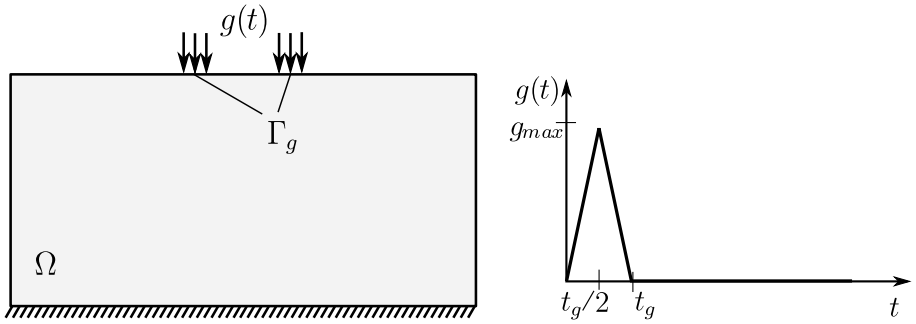

(a) Problem geometry (b) Time-dependent external load

Figure 3: Example 1: Problem statement.

The problem geometry is the rectangular plate sketched in figure 3(a). The plate is initially at rest ($\mathbf{u}_0 = \mathbf{v}_0 = \mathbf{0}$) and loaded with the time dependent traction

$$\mathbf{g} = \begin{cases} -g(t)\mathbf{e}_2 & \text{on } \Gamma_g, \\ 0 & \text{elsewhere,} \end{cases} \tag{46}$$

where $\mathbf{e}_2 := (0, 1)$ and $g(t)$ is the impulsive time-dependent function defined in figure 3(b) with parameters $g_{\max} = 30$ Pa and $t_g = 0.005$ s. No body force is acting in this example ($\mathbf{f} = \mathbf{0}$).

Table 1 details the geometrical parameters and material data, where E and ν are the Young's modulus and Poisson's ratio respectively and the parameter ξ is the dimensionless damping factor. In the examples included here we take $a_1 = 0$, and its corresponding value is $\xi := \frac{1}{2}\omega_1 a_2$, see [45, 42]. Three different values of the viscosity parameter a_2 are considered. The solution of the problem consists of elastic waves propagating along the plate, see [45] for a qualitative description of the solution.

Table 1: Example 1: Problem parameterization

Geometry			Material properties		
Ω	$(-0.5, 0.5) \times (0, 0.5)$	m^2	E	$8/3$	Pa
Γ_g	$[(0.075, 0.125) \cup (-0.075, -0.125)] \times (0.5)$	m	ν	$1/3$	
T	0.25	s	ρ	1	$\mathrm{kg/m}^3$
			a_1	0	s
			a_2	$\{0, 10^{-4}, 10^{-2}\}$	s
			ξ	$\{0, 0.0247, 2.47\}$	%

In a first phase, the error estimate is analyzed for the scalar quantity of interest

$$s_T := (\rho \mathbf{q}_1, \dot{\mathbf{u}}(T)). \tag{47}$$

This quantity is a particular case of the quantities represented by the functional $L_1^{\mathcal{O}}$ presented in section 3.4. The quantity s_T is associated with the *exact* first eigenvector of the generalized eigenvalue problem (26) which is unknown. In the following, function $\mathbf{q}_1$ is replaced by a reference eigenvector $\mathbf{q}_1^{H,p+1}$ solution of the eigenvalue problem (26) in the discrete space $\boldsymbol{\mathcal{V}}_0^{H,p+1}$. The space $\boldsymbol{\mathcal{V}}_0^{H,p+1}$ is obtained increasing by one the interpolation order of $\boldsymbol{\mathcal{V}}_0^{H}$. In order to have a reference error to assess the effectivity of the presented error estimation approach, the *exact* solution $\mathbf{u}$ (which is also unknown) is replaced by an admissible reference solution computed using the space $\boldsymbol{\mathcal{V}}_0^{H,p+1}$ and a time step length $\Delta t/2$. Note that the proposed approximations to $\mathbf{u}$ and $\mathbf{q}_1$ are discretization-dependent.

The numerical solution of the problem $\hat{\mathbf{u}}$ is computed for three different meshes and four time step lengths. Table 2 contains detailed information on both the space and time discretizations. The element size H appearing in table 2 is defined as the size of the smallest triangular element, where the size of a triangular element is taken as the diameter of its inscribed circle. The coarsest mesh (referred as mesh id. 1) is plotted in figure 4. Note that only half of the computational domain Ω is discretized by introducing suitable symmetry conditions.

Each computational mesh provides the approximation to the quantity of interest

$$\hat{s}_T = (\rho \mathbf{q}_1, \dot{\hat{\mathbf{u}}}(T)). \tag{48}$$

The error $s_T^{\mathrm{e}} = s_T - \hat{s}_T$ is computed using the reference value for s_T previously defined. On the other hand, the estimate $\tilde{s}_T^{\mathrm{e}}$ is computed following section 3.4. Note that for the quantity of interest introduced in (47) only one vibration mode ($M = 1$) is required to build the enhanced adjoint approximation $\tilde{\mathbf{u}}^{\mathrm{d}}$.

Figures 5 and 6 show the space and time convergence of the errors s_T^{e} and $\tilde{s}_T^{\mathrm{e}}$ for the three different values of the damping parameter a_2 given in table 1. The space convergence curves are

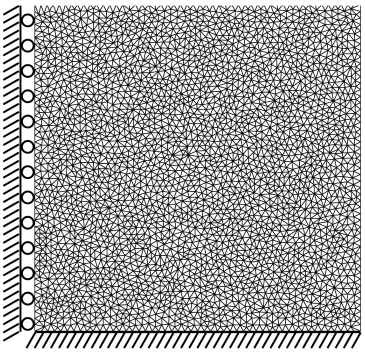

Figure 4: Example 1: Computational domain and coarsest computational mesh.

Table 2: Example 1: Space and time discretizations

Mesh id.	N_{nod}	# Elements	Type	H [m]
1	3051	5899	Triangle	$3.2 \cdot 10^{-3}$
2	12000	23596	”	$1.6 \cdot 10^{-3}$
3	47595	94384	”	$7.9 \cdot 10^{-4}$

Time step id.	# steps	Δt [s]
1	100	$2.5 \cdot 10^{-3}$
2	200	$1.3 \cdot 10^{-3}$
3	400	$6.2 \cdot 10^{-4}$
4	800	$3.1 \cdot 10^{-4}$

obtained keeping constant the time step length, $\Delta t = 6.2 \cdot 10^{-4}$ s, whereas the time convergence curves are obtained keeping constant the space discretization, i.e. using meshes id. 1 and 3 respectively.

Figure 5 shows that he estimate $\tilde{s}_T^{\text{e}}$ is in very good agreement with the reference error s_T^{e}. The optimal convergence rate for quantities of interest is two times the rate for the energy norm. That is, the error in the quantity of interest converges as $\mathcal{O}(H^2)$, see [59]. Note that the optimal space convergence rate is achieved both for $\tilde{s}_T^{\text{e}}$ and s_T^{e}.

Note in figure 6 that the time convergence plots rapidly converge to a constant value which is the committed space discretization error. Thus, the time discretization errors of $\tilde{s}_T^{\text{e}}$ and s_T^{e} are very small when compared to the space discretization errors. Even for the coarser mesh, the reduction of the time step does not vary the accuracy of the approximations.

Figures 5 and 6 show that the effectivities of the estimate $\tilde{s}_T^{\text{e}}$ is qualitatively the same for all the values of the damping parameter a_2, even in the limit case $a_2 = 0$. Thus, the presented technique is robust with respect to the damping parameter. Recall that the same behavior is not observed when dealing with error estimation techniques providing error bounds which effectivities degenerate as the amount of damping tends to zero, see [41, 42, 43, 44, 45]. In fact, existing techniques providing error bounds in energy norms or in quantities of interest can not even deal with the case $a_2 = 0$.

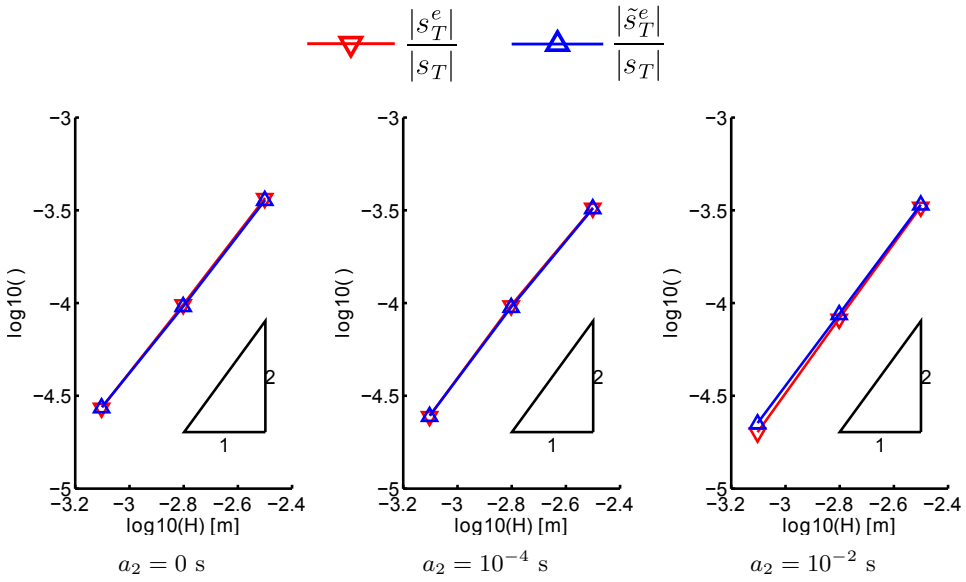

Figure 5: Example 1: Evolution of the relative error along a uniform H refinement process, for three values of the viscosity parameter a_2. Exact (reference) values described by the red triangles pointing downwards and estimated values described by the blue triangles pointing upwards. The results are computed with a constant time step length $\Delta t = 6.2 \cdot 10^{-4}$ s.

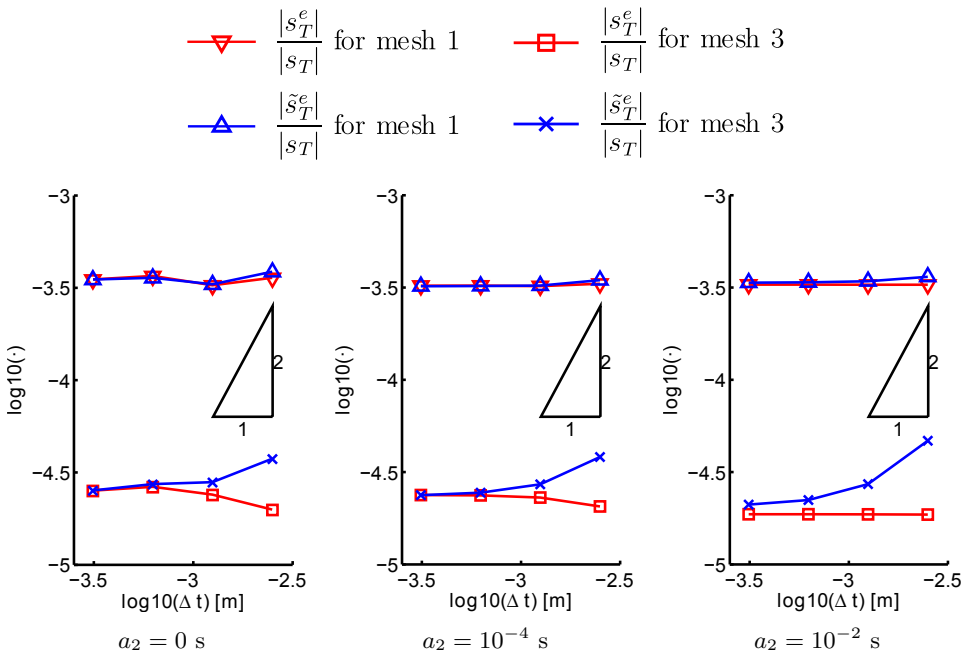

Figure 6: Example 1: Evolution of the relative error along a uniform Δt refinement process, for three values of the viscosity parameter a_2. Exact (reference) values described by the red triangles pointing downwards (mesh 1) and squares (mesh 3) and estimated values described by the blue triangles pointing upwards (mesh 1) and crosses (mesh 3).

A related timeline-dependent quantity is considered also for this example,

$$s(t) = (\rho \mathbf{q}_1, \dot{\mathbf{u}}(t)).$$

Figure 7 shows the reference and approximated timeline quantities $s(t)$ and $\hat{s}(t) := (\rho \mathbf{q}_1, \dot{\hat{\mathbf{u}}}(t))$ and the reference and estimated errors $s^e(t)$ and $\hat{s}^e(t)$ for mesh id. 1 and time step id. 3, see table 2. As in the scalar case, the proposed estimate $\tilde{s}^{\mathrm{e}}(t)$ is really close to the reference value $s^{\mathrm{e}}(t)$ in all cases, also for $a_2 = 0$. It can be observed that, in this example, the quantity of interest associated to the lowest eigenvector $\mathbf{q}_1$ is nearly unaffected by the change in the damping coefficient a_2. However, the time dependent errors $s^{\mathrm{e}}(t)$ and its approximations $\tilde{s}^{\mathrm{e}}(t)$ are smoothed out as the coefficient a_2 increases.

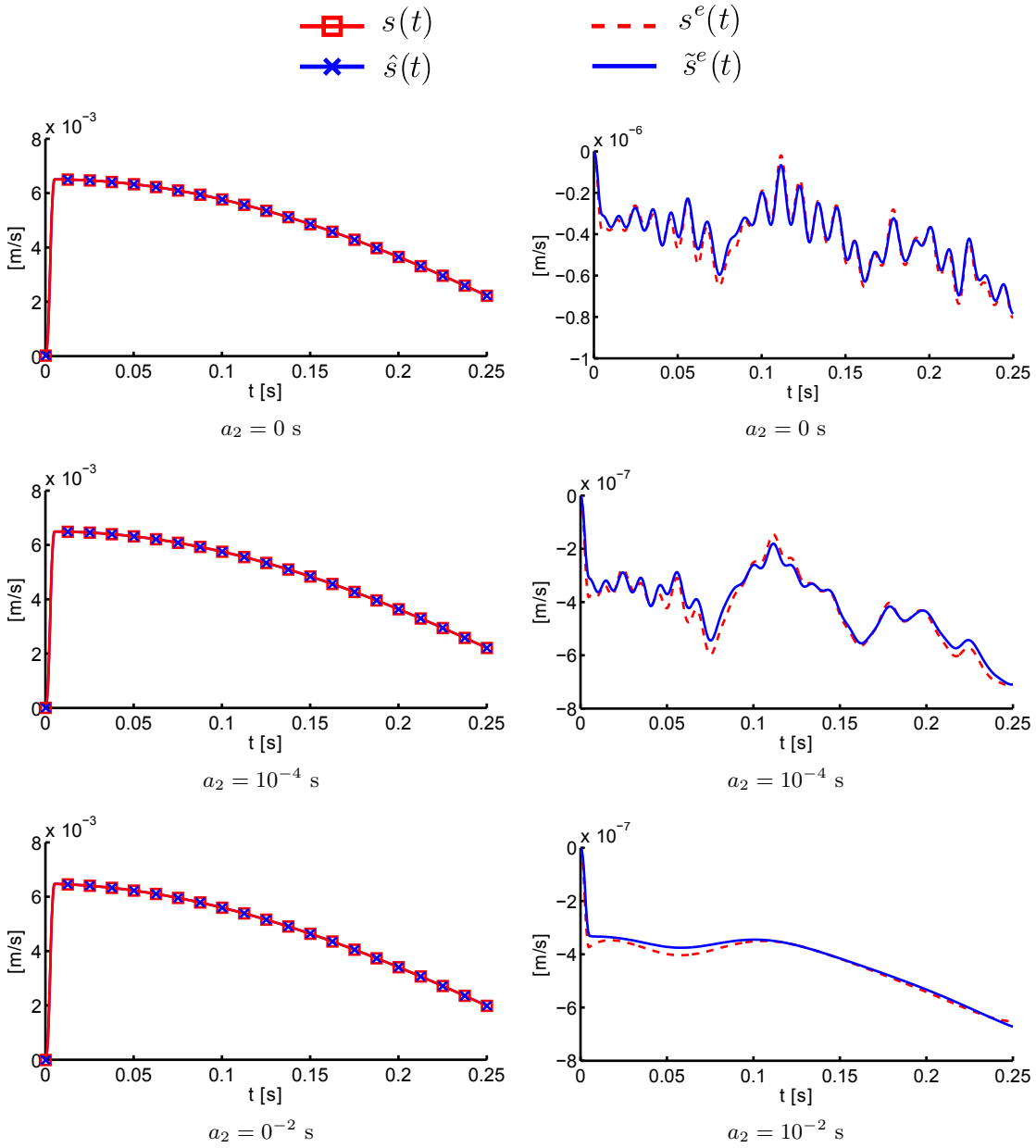

Figure 7: Example 1: Approximated and reference timeline-dependent quantity (left) and estimated and reference errors in the timeline-dependent quantity (right) for the three values of the damping parameter a_2 ($a_2 = 0\,$s, top; $a_2 = 10^{-2}$s, center; $a_2 = 10^{-4}$s, bottom).

5.2 Example 2

Consider the structure given in figure 8(a). The structure is initially at rest ($\mathbf{u}_0 = \mathbf{v}_0 = \mathbf{0}$), clamped at the supports and subjected to the time-dependent traction

$$\mathbf{g} = \begin{cases} g(t)\mathbf{e}_1 & \text{on } \Gamma_g, \\ 0 & \text{elsewhere.} \end{cases}$$

The set Γ_g is the region of the Neumann boundary where the load is applied, $\mathbf{e}_1 := (1, 0)$ is the first cartesian unit vector and function $g(t)$ describes the time evolution of $\mathbf{g}$ given in figure 8(b). The traction $\mathbf{g}$ is the only external loading in this example (that is $\mathbf{f} = \mathbf{0}$). Other material and geometric parameters univocally defining the problem are reported in table 3.

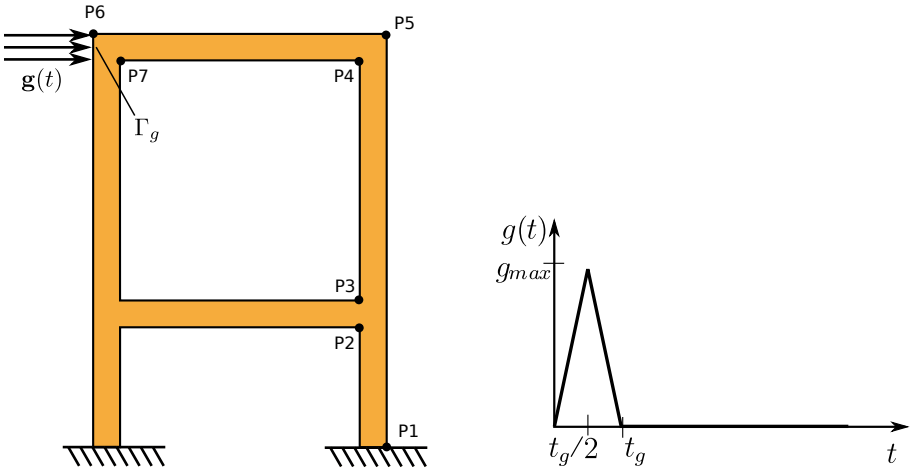

(a) Problem geometry (b) Time dependent loading at Γ_g

Figure 8: Example 2: Problem statement.

Table 3: Example 2: Problem parameterization

Geometry (data in m)	Physical properties
$P_1 := (0.55, 0.00)$	$E = 2 \cdot 10^{11}$ Pa
$P_2 := (0.45, 0.45)$	$\nu = 0.2$
$P_3 := (0.45, 0.55)$	$\rho = 8 \cdot 10^3$ kg/m^3
$P_4 := (0.45, 1.45)$	$a_1 = 0$ s
$P_5 := (0.55, 1.55)$	$a_2 \in \{0, 1 \cdot 10^{-4}, 1 \cdot 10^{-3}\}$ s
$P_6 := (-0.55, 1.55)$	$\xi \in \{0, 1.75, 17.6\}$ %
$P_7 := (-0.45, 1.45)$	$T = 2 \cdot 10^{-3}$ s
$\Gamma_g := \{-0.55\} \times (1.45, 1.55)$	**External load**
	$g_{\max} = 10^8$ Pa
	$t_g = 2 \cdot 10^{-4}$ s

Consider the scalar quantities of interest

$$s_{u,T} := (\boldsymbol{\lambda}_{\mathrm{N}}^{\mathcal{O}}, \mathbf{u}(T))_{\Gamma_g} \text{ and } s_{v,T} := (\rho \mathbf{q}_1, \dot{\mathbf{u}}(T)),$$

where $\boldsymbol{\lambda}_{\mathrm{N}}^{\mathcal{O}} := \mathbf{e}_1/\mathrm{meas}(\Gamma_g)$. The quantity $s_{u,T}$ is an average of the horizontal displacements at the Neumann boundary Γ_g. Note that $s_{u,T}$ is a particular case of the quantities represented by the functional $L_2^{\mathcal{O}}(\cdot)$ introduced in section 3.4. On the other hand, $s_{v,T}$ is a weighted average of the velocities and it is a particular case of the quantities represented by $L_1^{\mathcal{O}}(\cdot)$ also introduced in section 3.4. The unknown values $s_{u,T}$ and $s_{v,T}$ are approximated in this example with an *overkill* discretization

$$s_{u,T} = (\boldsymbol{\lambda}_{\mathrm{N}}^{\mathcal{O}}, \mathbf{u}^{\mathrm{ovk}}(T))_{\Gamma_g} \text{ and } s_{v,T} = (\rho \mathbf{q}_1^{\mathrm{ovk}}, \dot{\mathbf{u}}^{\mathrm{ovk}}(T)),$$

where the superscript $()^{\mathrm{ovk}}$ refers to functions computed with the overkill discretization. The parameters of the overkill discretization are given in table 4. Note that only one overkill discretization is considered in this example which does not depend on the selected H-mesh.

The space and time discretizations used in this example are shown in table 4. The particular combinations of space-time discretizations which are actually taken into account are represented in figure 9. The same figure shows the coarsest finite element mesh (mesh id. 1). The other meshes are obtained as nested subdivisions of the coarser one.

Table 4: Example 2: Space and time discretizations.

Mesh id.	N_{dof}	# Elements	Type	p	H [m]
1	3394	2902	Triangle	1	$7.41 \cdot 10^{-3}$
2	12592	11608	”	1	$3.71 \cdot 10^{-3}$
3	48400	46432	”	1	$1.85 \cdot 10^{-3}$
ovk.	189664	185744	”	1	$9.26 \cdot 10^{-4}$

Time step id.	# steps	Δt [s]
1	100	$2.00 \cdot 10^{-5}$
2	200	$1.00 \cdot 10^{-5}$
3	400	$5.00 \cdot 10^{-6}$
4	800	$2.50 \cdot 10^{-6}$
ovk.	3200	$6.25 \cdot 10^{-7}$

The space-time discretization of the problem provides the approximation $\hat{s}_{u,T} = (\boldsymbol{\lambda}_{\mathrm{N}}^{\mathcal{O}}, \hat{\mathbf{u}}(T))_{\Gamma_g}$ and $\hat{s}_{v,T} = (\rho \mathbf{q}_1^H, \dot{\hat{\mathbf{u}}}(T))$ to the exact quantities of interest $s_{u,T}$ and $s_{v,T}$ respectively. Note that the approximation $\hat{s}_{v,T}$ is computed using the discrete eigenvector $\mathbf{q}_1^H$ instead of the exact one $\mathbf{q}_1$ (approached by $\mathbf{q}_1^{\mathrm{ovk}}$). The reason is that $(\rho \mathbf{q}_1^H, \dot{\hat{\mathbf{u}}}(T))$ provides a very good approximation to $(\rho \mathbf{q}_1^{\mathrm{ovk}}, \dot{\hat{\mathbf{u}}}(T))$ in this example.

The estimates $\tilde{s}_{u,T}^{\mathrm{e}} \approx s_{u,T}^{\mathrm{e}} := s_{u,T} - \hat{s}_{u,T}$ and $\tilde{s}_{v,T}^{\mathrm{e}} \approx s_{v,T}^{\mathrm{e}} := s_{v,T} - \hat{s}_{v,T}$ are computed following the strategy of section 3. As mentioned in section 3.4, the computation of the displacement estimate $\tilde{s}_{u,T}^{\mathrm{e}}$, requires introducing the auxiliary linear elasticity problem

$$a(\mathbf{u}^{\mathcal{O}}, \mathbf{w}) = (\boldsymbol{\lambda}_{\mathrm{N}}^{\mathcal{O}}, \mathbf{w})_{\Gamma_g} \quad \forall \mathbf{v} \in \boldsymbol{\mathcal{V}}_0, \tag{49}$$

which allows rewriting the quantity $s_{u,T}$ as

$$s_{u,T} = a(\mathbf{u}^{\mathcal{O}}, \hat{\mathbf{u}}(T)).$$

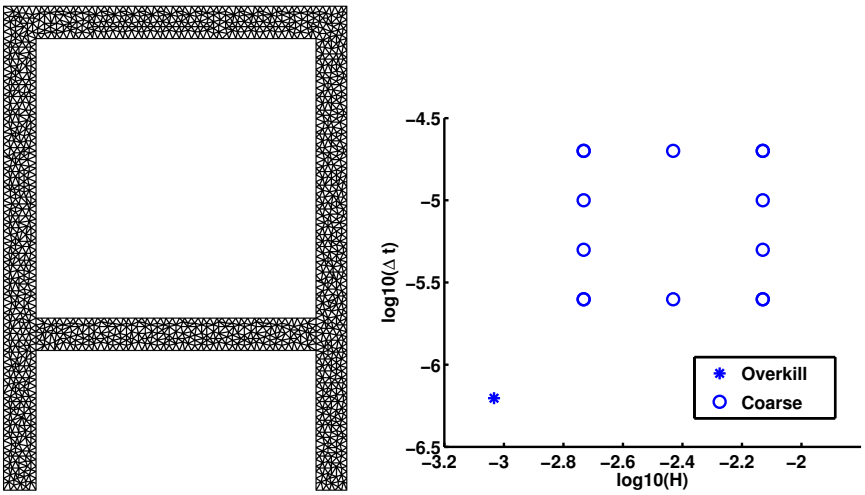

Figure 9: Example 2: Coarsest finite element mesh used in this example (left). Element sizes and time step lengths used in the example (right).

Recall that, computing the enhanced adjoint solution $\tilde{\mathbf{u}}^{\mathrm{d}}$ for this quantity requires finding the values $\tilde{u}_i$, $i = 1, \ldots, M$ such that

$$\mathbf{u}^{\mathcal{O}} \approx \sum_{i=1}^{M} \tilde{u}_i \tilde{\mathbf{q}}_i.$$

Since $\mathbf{u}^{\mathcal{O}}$ is not available, it is replaced by an enhanced field $\tilde{\mathbf{u}}^{\mathcal{O}}$ obtained by post-processing $\mathbf{u}^{\mathcal{O},H}$, the finite element approximation of the elasticity problem (49), using the technique explained in section 3.3. The values $\tilde{u}_i$ are computed using three different strategies. The first one is to recover the coefficients $\tilde{u}_i^1$ using the least squares technique described in remark 5. The second assumes that the recovered eigenvectors are orthonormal and recovers the coefficients as $\tilde{u}_i^2 = (\rho\tilde{\mathbf{u}}^{\mathcal{O}}, \tilde{\mathbf{q}}_i)$. Finally, the third strategy uses the original orthonormal eigenvectors $\mathbf{q}_i^H$, $\tilde{u}_i^3 = (\rho\mathbf{u}^{\mathcal{O},H}, \tilde{\mathbf{q}}_i^H)$. Figure 10 shows that the least squares technique allows to properly recover the extractor $\tilde{\mathbf{u}}^{\mathcal{O}}$ by increasing the number of modes M in the decomposition. The two cheaper alternatives (2 and 3) behave very differently. Assuming that the recovered eigenvectors behave like an orthonormal basis, provide non-converging approximations to the extractor $\tilde{\mathbf{u}}^{\mathcal{O}}$. Strategies 1 and 3 provide very close results. The third strategy is considered in this example to compute the values $\tilde{u}_i$. The default number of vibration modes used to compute the estimate $\tilde{s}^{\mathrm{e}}_{u,T}$ in this example is $M = 60$.

Figures 11 and 12 show the convergence of the computed estimates $\tilde{s}^{\mathrm{e}}_{u,T}$ and $\tilde{s}^{\mathrm{e}}_{v,T}$ and of the overkill errors $s^{\mathrm{e}}_{u,T}$ and $s^{\mathrm{e}}_{v,T}$ with respect to the space and time discretizations, respectively, for two different values of the damping parameter a_2. The space convergence curves are obtained keeping the time discretization constant whereas the time convergence plots are obtained keeping the space discretization constant.

Figure 11 shows that the errors $\tilde{s}^{\mathrm{e}}_{v,T}$ and $s^{\mathrm{e}}_{v,T}$ converge at the optimal space convergence rate. On the other hand, the errors $\tilde{s}^{\mathrm{e}}_{u,T}$ and $s^{\mathrm{e}}_{u,T}$ converge at the optimal rate for all cases except one ($a2 = 0$ s and $\Delta t = 2.00 \cdot 10^{-5}$ s). In this case, the time discretization error is dominant with respect to the spatial error, and thus refining the spatial mesh does not yield any gain in accuracy. In the other cases, the space integration error is dominant and therefore the optimal space convergence is achieved.

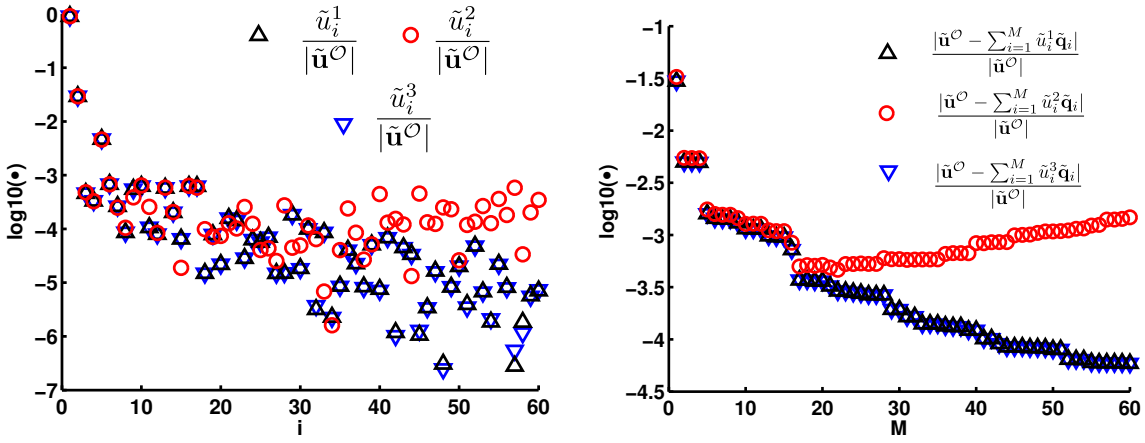

Figure 10: Example 2: Comparison of three different strategies providing the values $\tilde{u}_i$, $i = 1, \ldots, M$ (left). Convergence of the three different representations of the extractor $\tilde{\mathbf{u}}^{\mathcal{O}}$ in the recovered eigenvector basis $\{\tilde{\mathbf{q}}_i\}_{i=1,\ldots,M}$ (right).

Figure 12 shows that the optimal time convergence rate is achieved for the values $\tilde{s}^{\mathrm{e}}_{u,T}$ and $s^{\mathrm{e}}_{u,T}$ computed with $H = 7.4 \cdot 10^{-3}$ m and $a_2 = 0$. That is the only case where the time discretization errors are dominant. In the other, cases the space discretization error is dominant and, therefore the time convergence stagnates to a constant value.

Consequently, figures 11 and 12 show that the estimates $\tilde{s}^{\mathrm{e}}_{u,T}$ and $\tilde{s}^{\mathrm{e}}_{v,T}$ properly assess the error associated with both the spatial and time discretizations.

Table 5 shows the effectivities of the estimates showed in Figures 11 and 12. Note that the effectivities for the estimate $\tilde{s}^{\mathrm{e}}_{v,T}$ are better than for $\tilde{s}^{e}_{u,T}$. That is because $\tilde{s}^{e}_{u,T}$ has a truncation error associated with the number of vibration modes M whereas $\tilde{s}^{e}_{v,T}$ only requires one vibration mode ($M = 1$) and therefore has no truncation error. The effectivities for the estimate $\tilde{s}^{\mathrm{e}}_{u,T}$ are better for the high values of the viscosity parameter a_2. That is because when the viscosity is high, the high frequencies of the problem are damped, and therefore the truncation error associated with M becomes less relevant. However, the estimates $\tilde{s}^{\mathrm{e}}_{u,T}$ and $\tilde{s}^{e}_{v,T}$ give accurate error approximations regardless of the amount of damping. This is a major difference with respect to the estimates [42, 45] furnishing bounds of the error which are only applicable for a non-zero amount of dissipation and which strongly degenerate as the dissipation vanishes.

In order to analyze the recovery procedure for the vibration modes, the effectivity of the postprocessed pair $(\tilde{\omega}_i, \tilde{\mathbf{q}}_i)$ is assessed comparing them with the pair $(\omega_i^{H,p+1}, \mathbf{q}_i^{H,p+1})$ solution of the eigenvalue problem (20) in the space $\boldsymbol{\mathcal{V}}_0^{H,p+1}$. The effectivity of the finite element and enhanced eigenmodes are quantified by the indicators

$$\eta_i = \frac{\omega_i^H}{\omega_i^{H,p+1}} \quad \text{and} \quad \tilde{\eta}_i = \frac{\tilde{\omega}_i}{\omega_i^{H,p+1}}.$$

Table 6 shows the computed eigenvalues in the coarse mesh ω_i^H, the recovered $\tilde{\omega}_i$ and the reference ones $\omega_i^{H,p+1}$, along with the computed effectivities η_i and $\tilde{\eta}_i$ for several eigemodes. Note that the recovered eigenpairs are in very good agreement with the reference values. Thus, the use of the simple and cheap recovery procedure allows considerably improving the accuracy of the discrete eigenvalues ω_i^H.

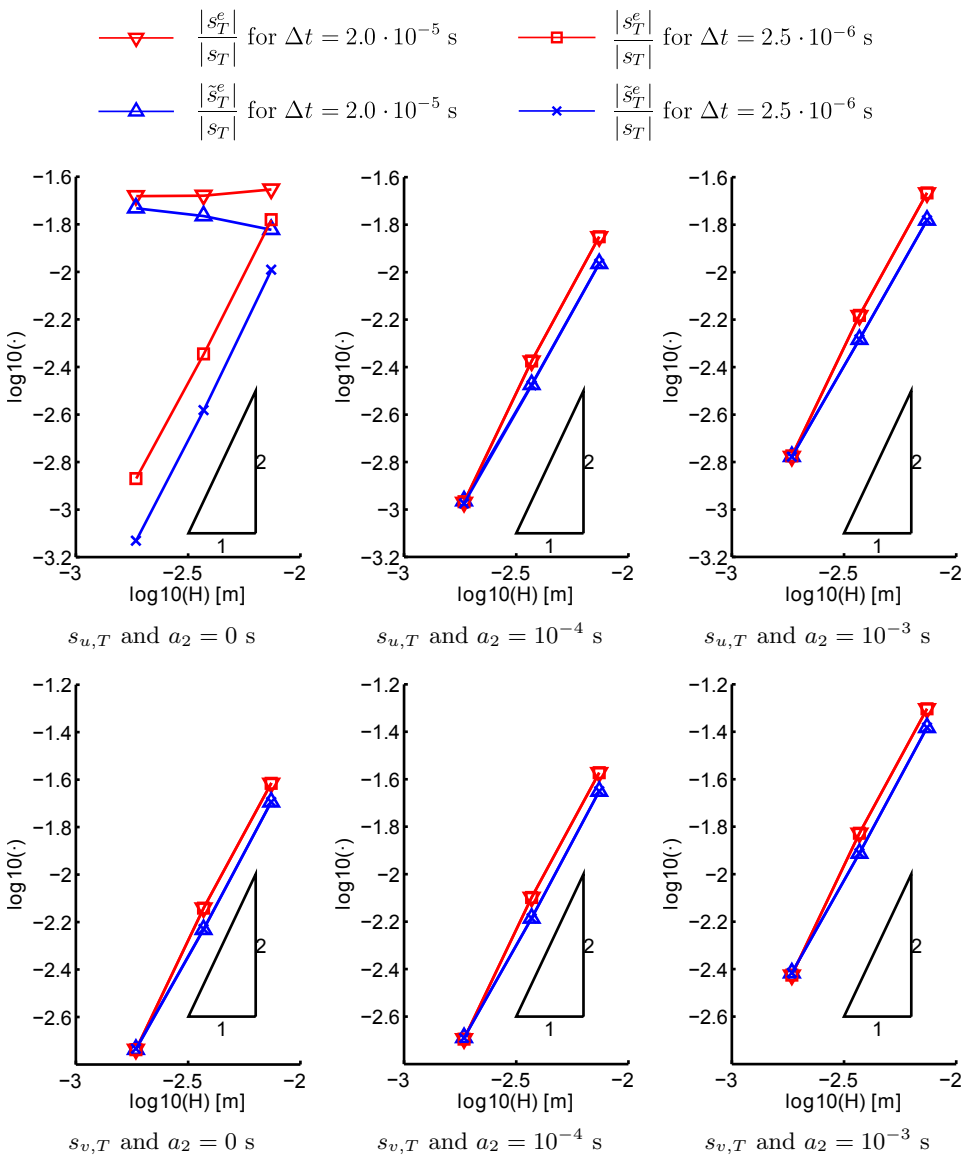

Figure 11: Example 2: Evolution of the relative error along a uniform H refinement process, for three values of the viscosity parameter a_2. Exact (overkill) values described by the red triangles pointing downwards ($\Delta t = 2.0 \cdot 10^{-5}$ s) and red squares ($\Delta t = 2.5 \cdot 10^{-6}$ s) and estimated values described by the blue triangles pointing upwards ($\Delta t = 2.0 \cdot 10^{-5}$ s) and blue crosses ($\Delta t = 2.5 \cdot 10^{-6}$ s).

Consider now the timeline-dependent quantities associated with $s_{u,T}$ and $s_{v,T}$, namely

$$s_u(t) = (\boldsymbol{\lambda}_{\mathrm{N}}^{\mathcal{O}}, \mathbf{u}(t))_{\Gamma_g} \text{ and } s_v(t), = (\rho \mathbf{q}_1, \dot{\mathbf{u}}(t)).$$

The problem discretization provides the approximations

$$\hat{s}_u(t) = (\boldsymbol{\lambda}_{\mathrm{N}}^{\mathcal{O}}, \hat{\mathbf{u}}(t))_{\Gamma_g} \text{ and } \hat{s}_v(t) = (\rho \mathbf{q}_1^H, \dot{\hat{\mathbf{u}}}(t)).$$

Figure 13 plots the values of the *exact* quantities of interest $s_u(t)$ and $s_v(t)$ computed using the overkill mesh and the approximations $\hat{s}_u(t)$ and $\hat{s}_v(t)$ for the three different values of the

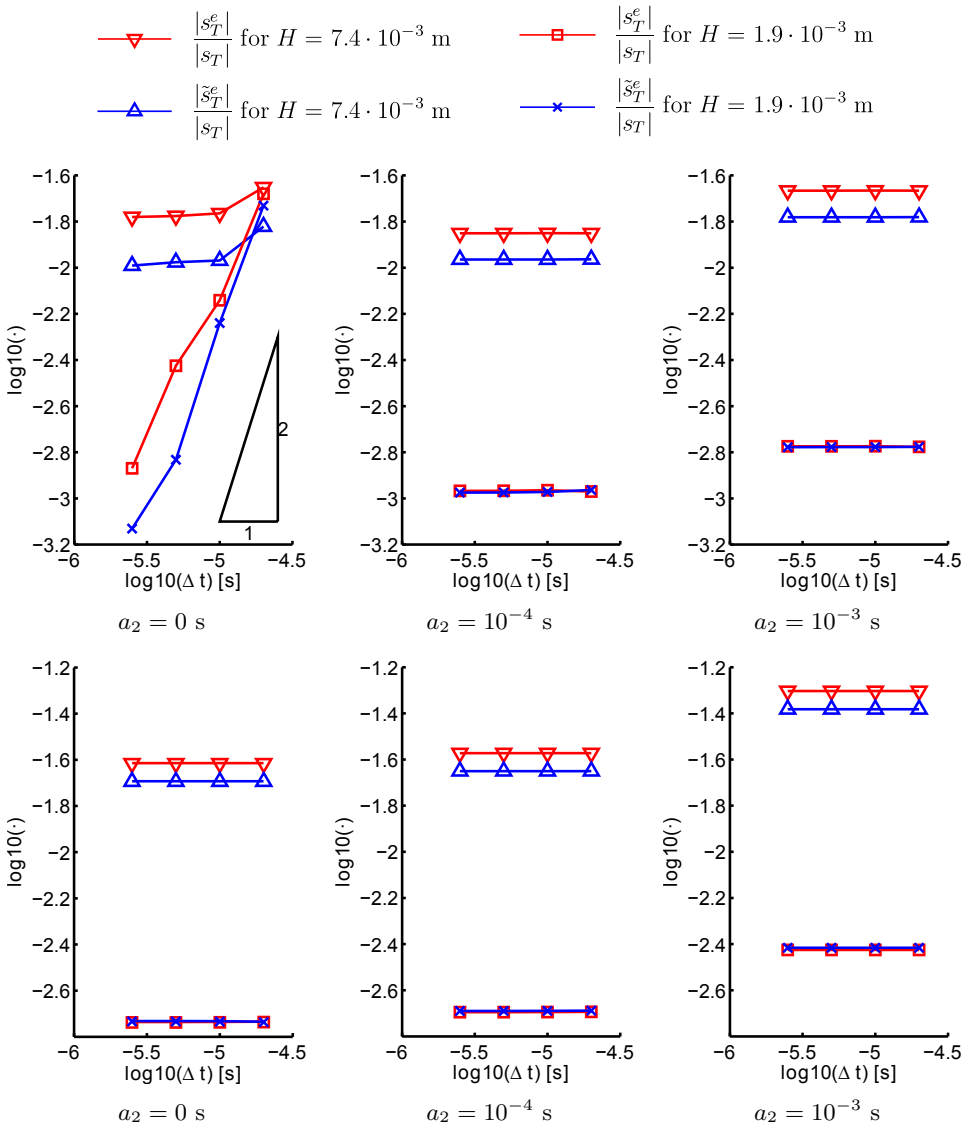

Figure 12: Example 2: Evolution of the relative error along a uniform Δt refinement process, for three values of the viscosity parameter a_2. Exact (overkill) values described by the red triangles pointing downwards ($H = 7.4 \cdot 10^{-3}$ m) and red squares ($H = 1.9 \cdot 10^{-3}$ m) and estimated values described by the blue triangles pointing upwards ($H = 7.4 \cdot 10^{-3}$ m) and blue crosses ($H = 1.9 \cdot 10^{-3}$ m).

parameter a_2. Note that, the approximations $\hat{s}_u(t)$ and $\hat{s}_v(t)$ are in very good agreement with the exact ones $s_u(t)$ and $s_v(t)$.

Figure 14 shows the evolution of the errors $s_u^{\mathrm{e}}(t) = s_u(t) - \hat{s}_u(t)$ and $s_v^{\mathrm{e}}(t) = s_v(t) - \hat{s}_v(t)$ jointly with the assessed errors $\tilde{s}_u^{\mathrm{e}}(t)$ and $\tilde{s}_v^{\mathrm{e}}(t)$ for three meshes keeping constant $\Delta t = 2.0 \cdot 10^{-5}$ s and $a_2 = 0$ s. For both quantities of interest, the *exact* errors $s_u^{\mathrm{e}}(t)$ and $s_v^{\mathrm{e}}(t)$ are fairly well approximated with the estimates $\tilde{s}_u^{\mathrm{e}}(t)$ and $\tilde{s}_v^{\mathrm{e}}(t)$. Note that the quality of the estimate $\tilde{s}_v^{\mathrm{e}}(t)$ improves as the element size is decreased. This is because the eigenpair $(\omega_1^H, \mathbf{q}_1^H)$ is better captured by the fine mesh than for the coarser ones. On the other hand, the estimate $\tilde{s}_u^{\mathrm{e}}(t)$ reproduces the average behavior of the error $s_u^{\mathrm{e}}(t)$. However, more vibration modes should be

Table 5: Example 2: Effectivities of the error estimates.

H [m]	Δt [s]	$a_2 = 0$ s $\frac{\tilde{s}^{\mathrm{e}}_{u,T}}{s^{\mathrm{e}}_{u,T}}$	$a_2 = 0$ s $\frac{\tilde{s}^{\mathrm{e}}_{v,T}}{s^{\mathrm{e}}_{v,T}}$	$a_2 = 1 \cdot 10^{-4}$ s $\frac{\tilde{s}^{\mathrm{e}}_{u,T}}{s^{\mathrm{e}}_{u,T}}$	$a_2 = 1 \cdot 10^{-4}$ s $\frac{\tilde{s}^{\mathrm{e}}_{v,T}}{s^{\mathrm{e}}_{v,T}}$	$a_2 = 1 \cdot 10^{-3}$ s $\frac{\tilde{s}^{\mathrm{e}}_{u,T}}{s^{\mathrm{e}}_{u,T}}$	$a_2 = 1 \cdot 10^{-3}$ s $\frac{\tilde{s}^{\mathrm{e}}_{v,T}}{s^{\mathrm{e}}_{v,T}}$
$7.41 \cdot 10^{-3}$	$2.0 \cdot 10^{-5}$	0.676	0.835	0.771	0.835	0.766	0.834
$7.41 \cdot 10^{-3}$	$1.0 \cdot 10^{-5}$	0.624	0.835	0.769	0.835	0.767	0.834
$7.41 \cdot 10^{-3}$	$5.0 \cdot 10^{-6}$	0.630	0.835	0.769	0.835	0.767	0.834
$7.41 \cdot 10^{-3}$	$2.5 \cdot 10^{-6}$	0.616	0.835	0.769	0.835	0.767	0.834
$1.85 \cdot 10^{-3}$	$2.0 \cdot 10^{-5}$	0.889	1.000	1.016	1.012	0.999	1.022
$1.85 \cdot 10^{-3}$	$1.0 \cdot 10^{-5}$	0.797	1.008	0.983	1.012	0.992	1.022
$1.85 \cdot 10^{-3}$	$5.0 \cdot 10^{-6}$	0.391	1.010	0.983	1.012	0.992	1.022
$1.85 \cdot 10^{-3}$	$2.5 \cdot 10^{-6}$	0.548	1.010	0.983	1.012	0.992	1.022
$7.41 \cdot 10^{-3}$	$2.0 \cdot 10^{-5}$	0.676	0.835	0.771	0.835	0.766	0.834
$3.70 \cdot 10^{-3}$	$2.0 \cdot 10^{-5}$	0.820	0.813	0.797	0.818	0.795	0.824
$1.85 \cdot 10^{-3}$	$2.0 \cdot 10^{-5}$	0.889	1.000	1.016	1.012	0.999	1.022
$7.41 \cdot 10^{-3}$	$2.5 \cdot 10^{-6}$	0.616	0.835	0.769	0.835	0.767	0.834
$3.70 \cdot 10^{-3}$	$2.5 \cdot 10^{-6}$	0.580	0.817	0.789	0.818	0.793	0.824
$1.85 \cdot 10^{-3}$	$2.5 \cdot 10^{-6}$	0.548	1.010	0.983	1.012	0.992	1.022

Table 6: Example 2: Effectivity of the recovered eigenfrequencies [rad/s]. The eigenvalues obtained using the overkill mesh are $\omega_1^{\mathrm{ovk}} = 3.3585 \cdot 10^2$, $\omega_{20}^{\mathrm{ovk}} = 1.4625 \cdot 10^4$, $\omega_{40}^{\mathrm{ovk}} = 3.8587 \cdot 10^4$ and $\omega_{60}^{\mathrm{ovk}} = 6.3211 \cdot 10^4$.

H [m]	i	ω_i^H	$\tilde{\omega}_i$	$\omega_i^{H,p+1}$	η_i	$\tilde{\eta}_i$
$7.41 \cdot 10^{-3}$	1	$3.5282 \cdot 10^2$	$3.3984 \cdot 10^2$	$3.3667 \cdot 10^2$	1.0480	1.0094
$7.41 \cdot 10^{-3}$	20	$1.5243 \cdot 10^4$	$1.4780 \cdot 10^4$	$1.4745 \cdot 10^4$	1.0338	1.0024
$7.41 \cdot 10^{-3}$	40	$4.0870 \cdot 10^4$	$3.9257 \cdot 10^4$	$3.9035 \cdot 10^4$	1.0470	1.0057
$7.41 \cdot 10^{-3}$	60	$6.7082 \cdot 10^4$	$6.5151 \cdot 10^4$	$6.4901 \cdot 10^4$	1.0336	1.0039
$3.71 \cdot 10^{-3}$	1	$3.4111 \cdot 10^2$	$3.3703 \cdot 10^2$	$3.3596 \cdot 10^2$	1.0153	1.0032
$3.71 \cdot 10^{-3}$	20	$1.4863 \cdot 10^4$	$1.4745 \cdot 10^4$	$1.4734 \cdot 10^4$	1.0088	1.0007
$3.71 \cdot 10^{-3}$	40	$3.9476 \cdot 10^4$	$3.9058 \cdot 10^4$	$3.9004 \cdot 10^4$	1.0121	1.0014
$3.71 \cdot 10^{-3}$	60	$6.5174 \cdot 10^4$	$6.4933 \cdot 10^4$	$6.4862 \cdot 10^4$	1.0048	1.0011
$1.85 \cdot 10^{-4}$	1	$3.3736 \cdot 10^2$	$3.3607 \cdot 10^2$	$3.3562 \cdot 10^2$	1.0052	1.0013
$1.85 \cdot 10^{-4}$	20	$1.4766 \cdot 10^4$	$1.4735 \cdot 10^4$	$1.4729 \cdot 10^4$	1.0025	1.0004
$1.85 \cdot 10^{-4}$	40	$3.9088 \cdot 10^4$	$3.9009 \cdot 10^4$	$3.8993 \cdot 10^4$	1.0024	1.0004
$1.85 \cdot 10^{-4}$	60	$6.4953 \cdot 10^4$	$6.4871 \cdot 10^4$	$6.4847 \cdot 10^4$	1.0016	1.0004

considered in computing $\tilde{s}^{\mathrm{e}}_u(t)$ to capture all the features.

Figure 15 shows the dependence of the error estimates $\tilde{s}^{\mathrm{e}}_u(t)$ on the number of vibrations modes M using mesh id. 2 and time step id. 4. The higher is M, the better $\tilde{s}^{\mathrm{e}}_u(t)$ approximates $s^{\mathrm{e}}_u(t)$. This is because the truncation error associated with M is reduced. On the other hand, the estimate is closer to the reference value as the damping parameter a_2 increases. That is because the high frequencies of the problem are damped and the truncation error becomes

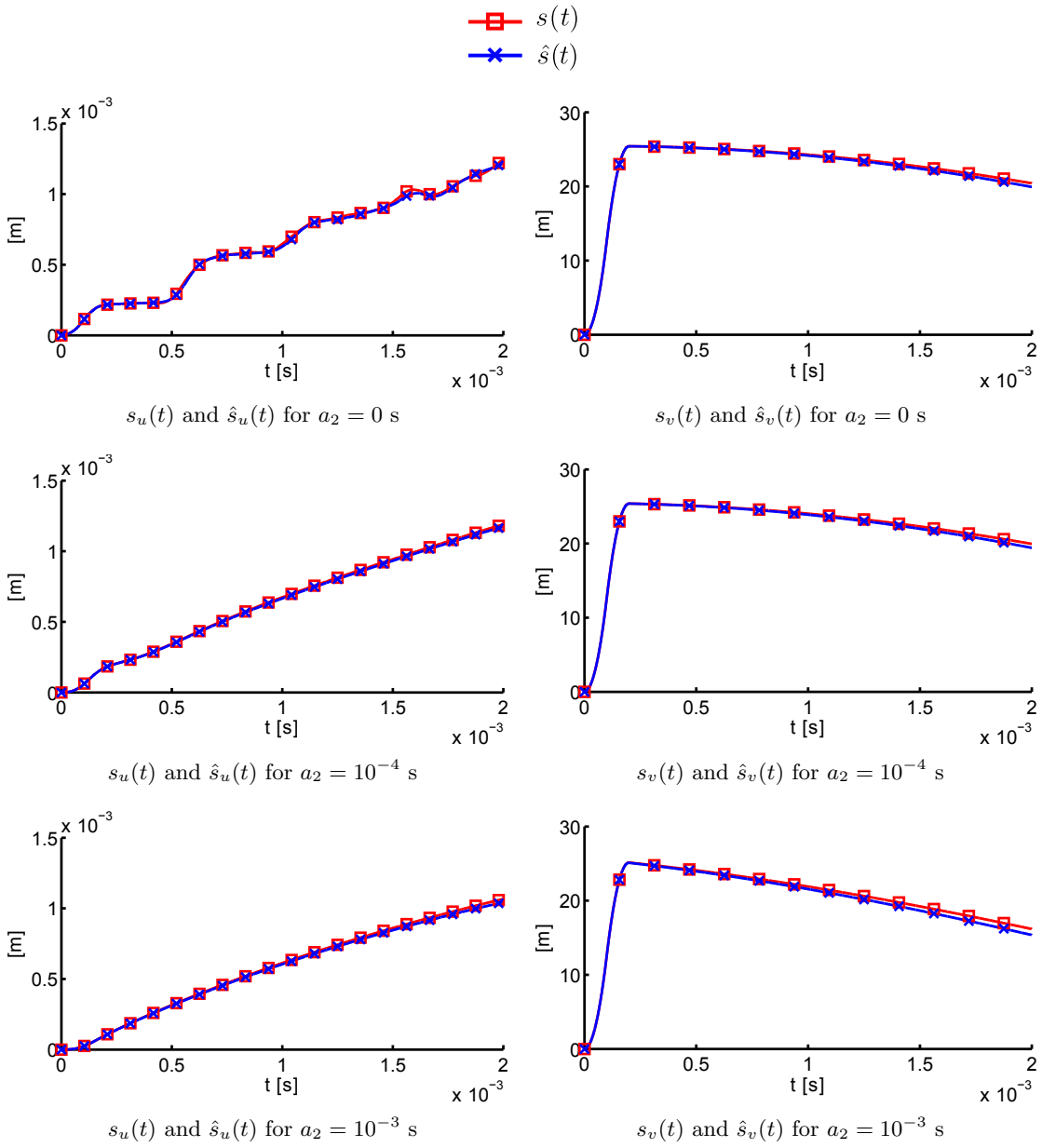

$s_u(t)$ and $\hat{s}_u(t)$ for $a_2 = 0$ s | $s_v(t)$ and $\hat{s}_v(t)$ for $a_2 = 0$ s

$s_u(t)$ and $\hat{s}_u(t)$ for $a_2 = 10^{-4}$ s | $s_v(t)$ and $\hat{s}_v(t)$ for $a_2 = 10^{-4}$ s

$s_u(t)$ and $\hat{s}_u(t)$ for $a_2 = 10^{-3}$ s | $s_v(t)$ and $\hat{s}_v(t)$ for $a_2 = 10^{-3}$ s

Figure 13: Example 2: Evolution of the timeline-dependent quantities $s_u(t)$ (left) and $s_v(t)$ (right) for three values of the parameter a_2. The approximate quantities $\hat{s}_u(t)$ and $\hat{s}_v(t)$ are computed with the discretization $H = 7.41 \cdot 10^{-3}$ m and $\Delta t = 2.0 \cdot 10^{-5}$ s.

less important. This is related to the parabolic character of the damping term. Note that in parabolic problems errors tend to dissipate along the time evolution, see [60].

As previously noted, the quality of the estimates clearly depends on the number of modes: as expected, when M increases and only the recovery procedure for each vibration mode affects the quality of the estimator. It is also worth noting that even though a fairly large number of modes are required to properly detect all the features of the evolution of the error in the quantity of interest, the shape of the curve is captured for reasonable low values of M. Finally, observe that, for the same number of modes, the estimate is closer to the reference value as

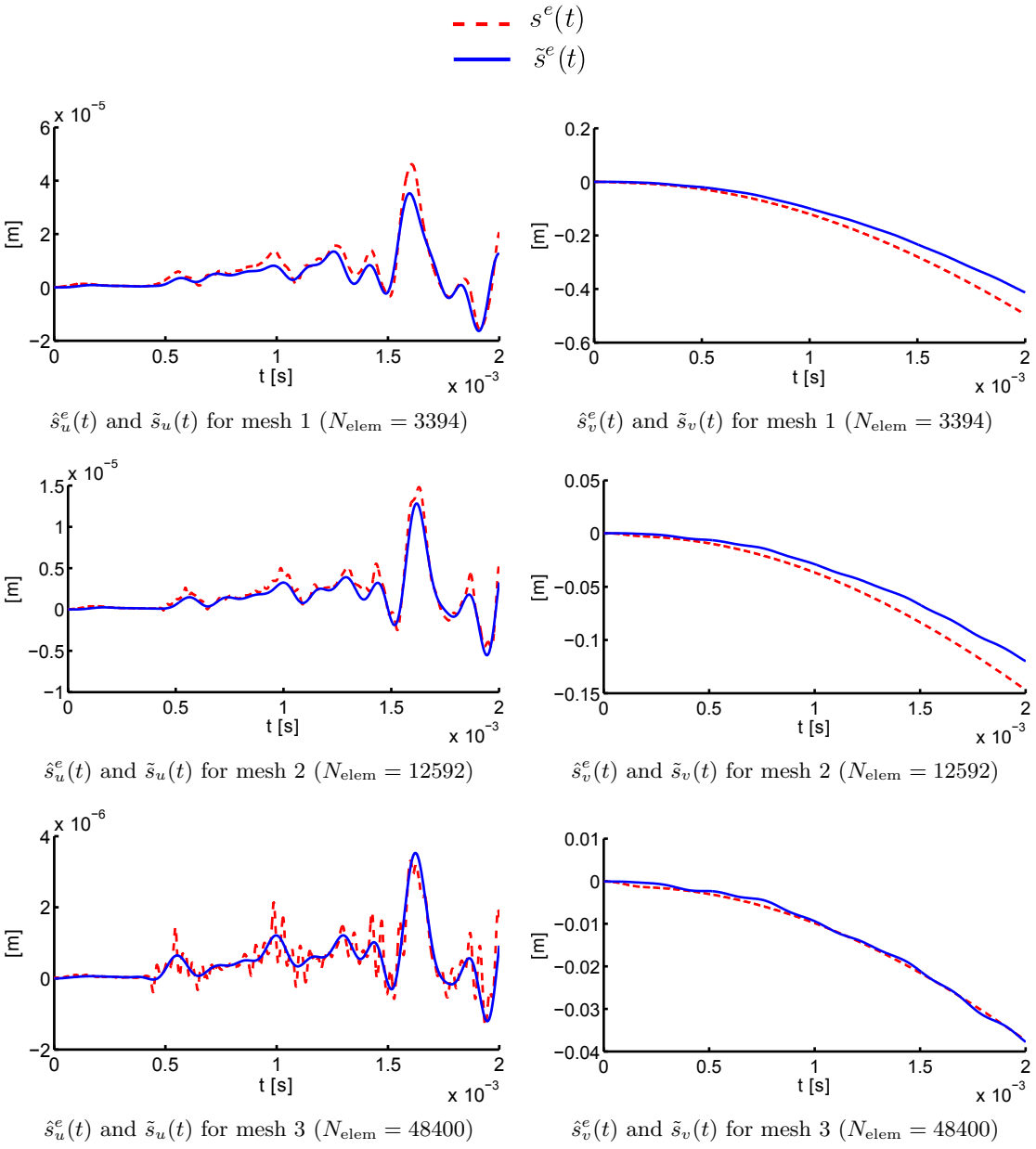

$\hat{s}^e_u(t)$ and $\tilde{s}_u(t)$ for mesh 1 ($N_{\text{elem}} = 3394$)

$\hat{s}^e_v(t)$ and $\tilde{s}_v(t)$ for mesh 1 ($N_{\text{elem}} = 3394$)

$\hat{s}^e_u(t)$ and $\tilde{s}_u(t)$ for mesh 2 ($N_{\text{elem}} = 12592$)

$\hat{s}^e_v(t)$ and $\tilde{s}_v(t)$ for mesh 2 ($N_{\text{elem}} = 12592$)

$\hat{s}^e_u(t)$ and $\tilde{s}_u(t)$ for mesh 3 ($N_{\text{elem}} = 48400$)

$\hat{s}^e_v(t)$ and $\tilde{s}_v(t)$ for mesh 3 ($N_{\text{elem}} = 48400$)

Figure 14: Example 2: Time evolution of the errors associated to $s_u(t)$ (left) and $s_v(t)$ (right) for the three computational meshes and keeping constant $\Delta t = 2.50 \cdot 10^{-6}$ s.

the damping parameter a_2 increases.

5.3 Example 3

The example presented here is similar to the previous one but increasing the structural complexity. The aim is to demonstrate that the proposed methodology is not limited to simple academic cases. This example is efficiently tackled with an affordable number of modes and computational resources.

Consider the structure defined in figure 16. The structure is initially at rest ($\mathbf{u}_0 = \mathbf{v}_0 = \mathbf{0}$) and

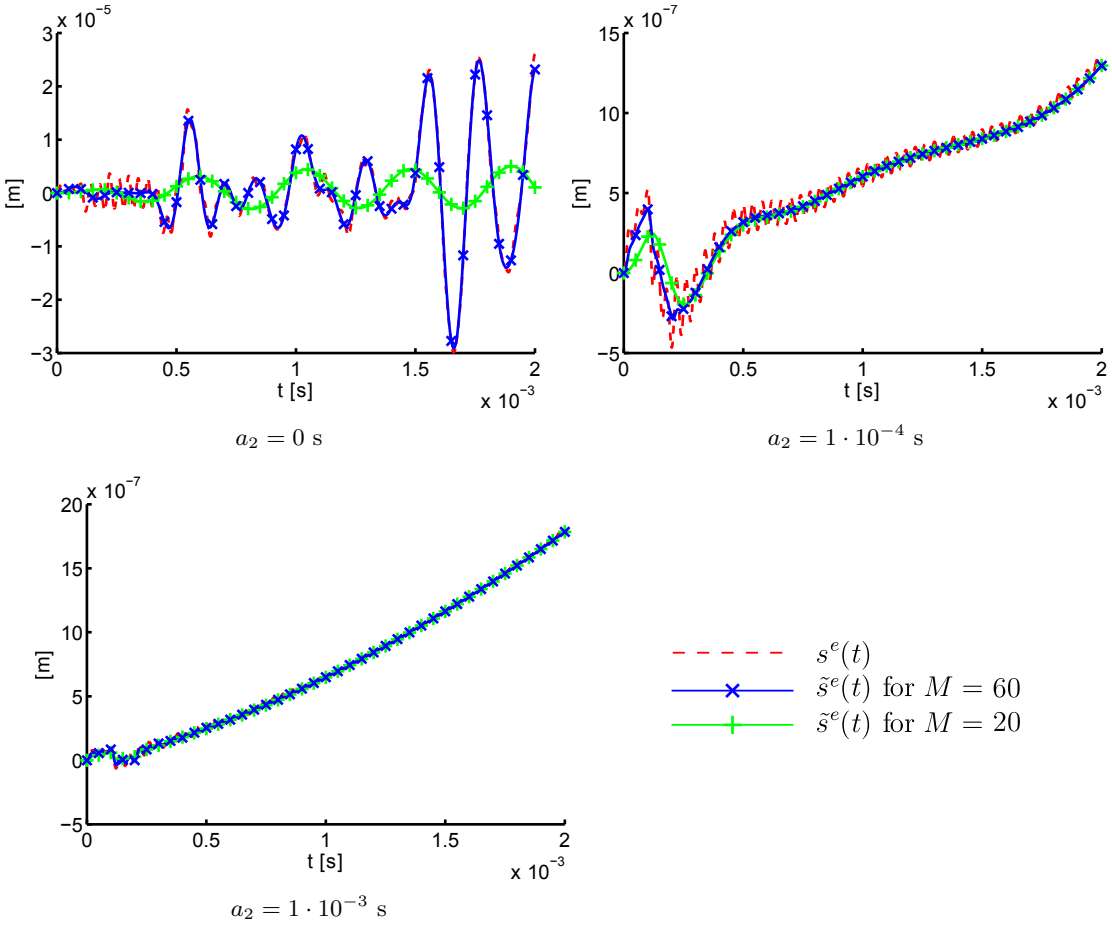

Figure 15: Example 2: Dependence of the assessed error $\tilde{s}^{\mathrm{e}}_u(t)$ on the number of vibration modes M for three values for the parameter a_2.

locally loaded with the time dependent traction

$$\mathbf{g}(\mathbf{x},t) := \begin{cases} g(t)\mathbf{e}_2 & \mathbf{x} \in \Gamma_g, \\ 0 & \mathbf{x} \in \Gamma_{\mathrm{N}} \setminus \Gamma_g. \end{cases}$$

The time weighting function $g(t)$ is also a triangular-shaped function like in figure 8(b). Table 7 contains all the parameters uniquely defining the problem. The response of the structure under the action of this load is shown in figure 17 for several simulation times.

In this example, the quantity of interest is an average of the vertical component of the displacements in the region Γ_g. Both the value of the average at the final simulation time and its evolution are considered, thus the following two quantities of interest are examined

$$s_T = (\boldsymbol{\lambda}_{\mathrm{N}}, \mathbf{u}(T))_{\Gamma_g} \quad \text{and} \quad s(t) = (\boldsymbol{\lambda}_{\mathrm{N}}, \mathbf{u}(t))_{\Gamma_g},$$

where $\lambda^{\mathcal{O}}_{\mathrm{N}} = \mathbf{e}_2/\mathrm{meas}(\Gamma_g)$. Note that these quantities coincide with $s_{u,T}$ and $s_u(t)$ of the previous example, but here the subscript u is omitted being the only quantities of interest under study. Recall that dealing with this quantity of interest requires introducing an auxiliary extractor $\mathbf{u}^{\mathcal{O}}$.

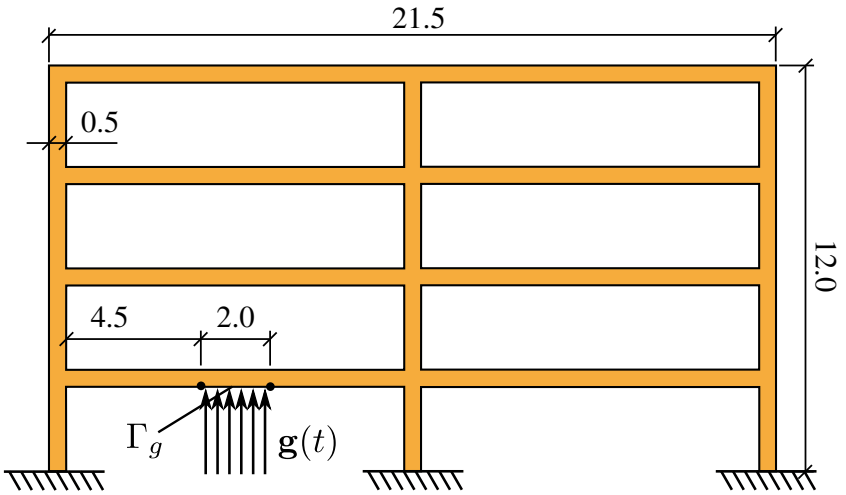

Figure 16: Example 3: Problem statement and geometry definition.

Table 7: Example 3: Problem parameterization

Physical properties	External load
$E = 2.7 \cdot 10^{10}$ Pa	$g_{\max} = 1 \cdot 10^{8}$ Pa
$\nu = 0.2$	$t_g = 1 \cdot 10^{-3}$ s
$\rho = 2.5 \cdot 10^{3}$ kg/m^3	
$a_1 = 0$ s	
$a_2 = 0$ s	
$T = 2 \cdot 10^{-2}$ s	

Several meshes and time step lengths are considered in order to evaluate the performance of the proposed estimates, see table 8. Table 8 also shows the parameters of the *overkill* discretization used to approximate the exact quantities s_T and $s(t)$.

Table 8: Example 3: Space and time discretizations

Mesh id.	N_{dof}	# Elements	Type	p	H [m]
1	2774	1876	Triangle	1	$1.15 \cdot 10^{-1}$
2	9310	7504	”	1	$5.77 \cdot 10^{-2}$
3	33638	30016	”	1	$2.89 \cdot 10^{-2}$
ovk.	127318	120064	”	1	$1.44 \cdot 10^{-2}$

Time step id.	# steps	Δt [s]
1	100	$1.00 \cdot 10^{-4}$
2	200	$5.00 \cdot 10^{-5}$
3	400	$2.50 \cdot 10^{-5}$
4	800	$1.25 \cdot 10^{-5}$
ovk.	3200	$6.25 \cdot 10^{-6}$

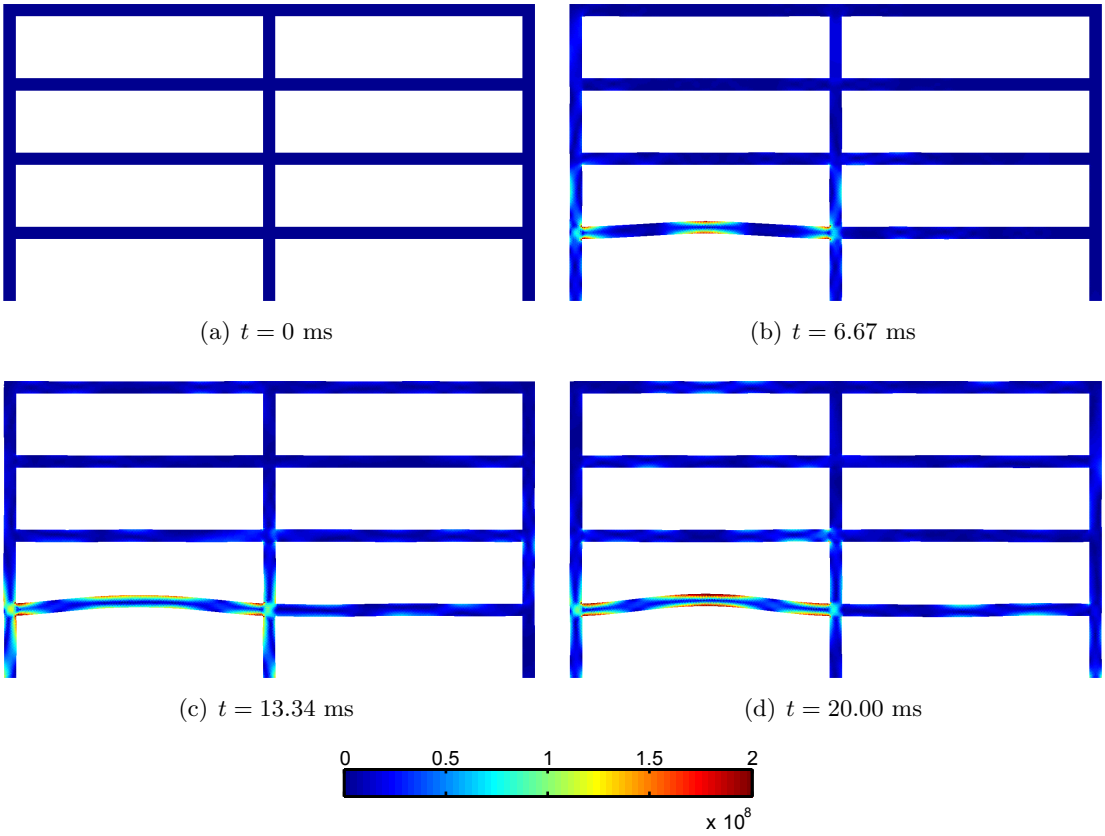

(a) $t = 0$ ms (b) $t = 6.67$ ms

(c) $t = 13.34$ ms (d) $t = 20.00$ ms

Figure 17: Example 3: Deformed geometry and von Mises criterion at several times. Solution computed using the mesh id. 3 and time step id. 4.

Using the same notation as in the previous examples, $\hat{s}_T$ and $\hat{s}(t)$ are the approximated quantities of interest and $\tilde{s}^{\mathrm{e}}_T$ and $\tilde{s}^{\mathrm{e}}(t)$ are the estimates of the *exact* errors $s^{\mathrm{e}}_T = s_T - \hat{s}_T$ and $s^{\mathrm{e}}(t) = s(t) - \hat{s}(t)$.

Figure 18 shows the space and time convergence of the estimate $\tilde{s}^{\mathrm{e}}_T$ and the overkill error s^{e}_T. The space convergence curves are obtained for a constant time step length of $\Delta t = 1.00 \cdot 10^{-4}$ s. The computed estimates are fairly close to the overkill values, and, its accuracy improves as the number of eigenmodes inreases. The results for $M = 40$ and $M = 60$ are quite close, and thus there is no significant gain in increasing the number of modes in the decomposition far beyond $M = 40$ since the performance of the error estimates is controlled by the recovery procedure. The time convergence plot is obtained using different time steps for a constant element size $H = 1.15 \cdot 10^{-1}$ m. In this case, the space discretization error is dominant with respect to the time discretization error, and therefore, reducing the time step length does not yield any gain in accuracy.

Table 9 shows the effectivities of the estimate $\tilde{s}^{\mathrm{e}}_T$ for different spatial mesh and number of eigenmodes. The quality of the estimate improves as the number of eigenmodes increases. However, a rough approximation of the error, which might be sufficient in some applications, is already obtained with $M = 20$ modes.

Figure 19 shows the evolution of the time-line dependent quantity of interest $s(t)$ along with the approximations $\hat{s}(t)$ computed using the three spatial meshes for a fixed time step $\Delta t = 10^{-4}$ s. As can be seen, the approximations of the quantity of interest converge to the *overkill* value

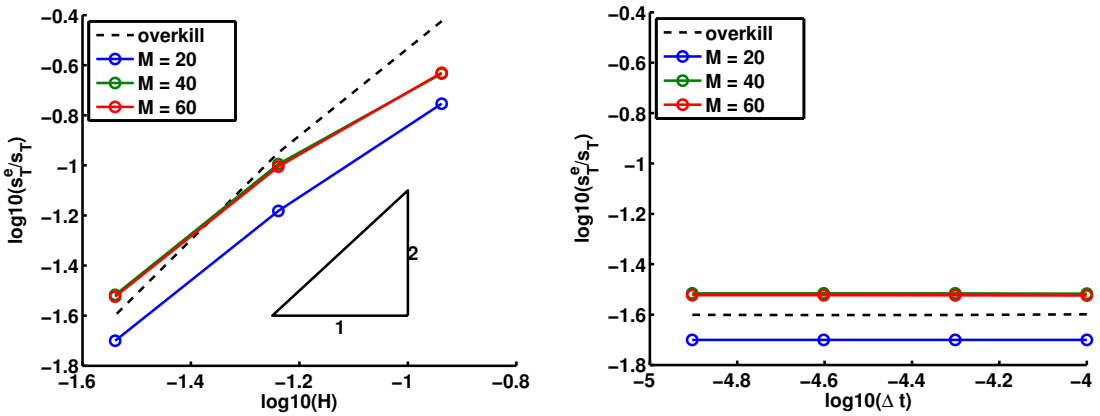

Figure 18: Example 3: Space (left) and time (right) convergence of estimate s_T^{e} and of the reference error $\tilde{s}_T^{\mathrm{e}}$ for different number of vibration modes M.

Table 9: Example 3: Computed effectivities

H [m]	Δt [s]	$\tilde{s}_T^{\mathrm{e}}/s_T^{\mathrm{e}}$		
		$M = 20$	$M = 40$	$M = 60$
$1.15 \cdot 10^{-1}$	$1.00 \cdot 10^{-4}$	0.468	0.617	0.622
$5.77 \cdot 10^{-2}$	$1.00 \cdot 10^{-4}$	0.586	0.900	0.879
$2.89 \cdot 10^{-2}$	$1.00 \cdot 10^{-4}$	0.792	1.207	1.188

as the mesh is refined, since the errors due to the time integration are negligible.

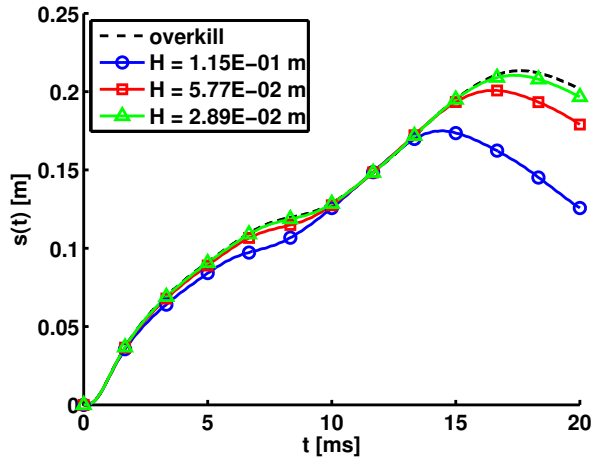

Figure 19: Example 3: Time evolution of the timeline-dependent quantity $s(t)$ and its approximation $\hat{s}(t)$ computed using the three different computational meshes for a fixed time step $\Delta t = 10^{-4}$ s.

Finally, figure 20 shows the computed estimates $\tilde{s}^{\mathrm{e}}(t)$ obtained varying the number of eigenmodes in the adjoint decomposition and for several meshes. As in the previous examples, the accuracy of the estimates increases with the number of considered eigenmodes. The estimate $\tilde{s}^{\mathrm{e}}(t)$, computed using $M = 20$ modes, reproduces the average behavior of $s^{\mathrm{e}}(t)$ whereas the

estimate $\tilde{s}^{\mathrm{e}}(t)$, computed using $M = 40$ or $M = 60$ modes, is a reasonably good approximation to $s^{\mathrm{e}}(t)$.

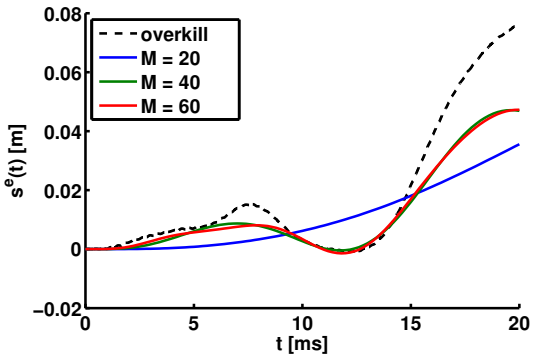

(a) $H = 1.15 \cdot 10^{-1}$ m

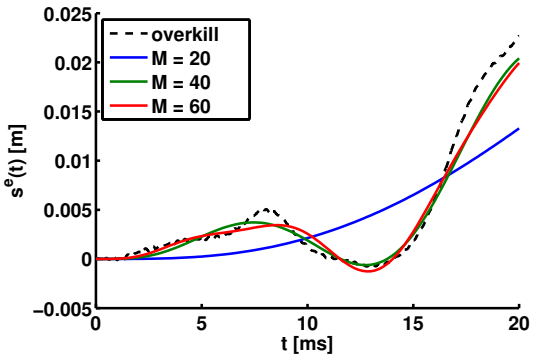

(b) $H = 5.77 \cdot 10^{-2}$ m

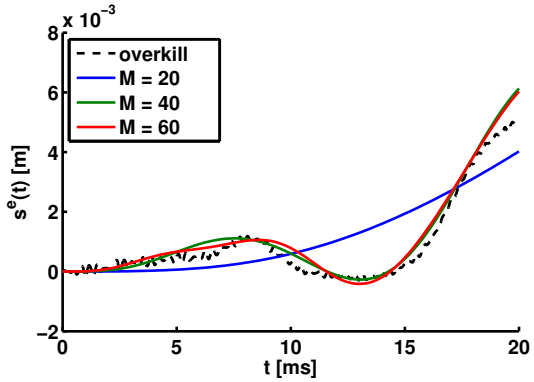

(c) $H = 2.89 \cdot 10^{-2}$ m

Figure 20: Example 3: Computed estimates $\tilde{s}^{\mathrm{e}}(t)$ using different number of eigenmodes and overkill error $s^{\mathrm{e}}(t)$ for the three computational meshes and a fixed time step $\Delta t = 10^{-4}$ s.

6 Conclusions

This article presents a new type of goal-oriented error estimates assessing the error in timeline-dependent quantities of interest. Timeline-dependent quantities are outputs of the solution describing the time evolution of some space-post-processed functional. Compared to the traditional scalar quantities of interest, this approach fits better the requirements of end-users in dynamic problems. Assessing the error in timeline-dependent quantities involves a family of infinite adjoint problems (one for each time instant in the time interval under consideration). However, all these adjoint problems are similar and they can be recovered from a common parent problem (associated with the a scalar quantity of interest) by means of a simple translation (shift) of the time variable.

The second novelty in this paper is the approximation of the adjoint problem using a decomposition into vibration modes. This allows efficiently precomputing and storing the adjoint solution. Thus, the error estimate is computed along the time integration of the original problem. This approach applies both for the scalar and timeline quantities, but it is specially indicated for the latter because it simplifies the implementation of the time shift.

The error estimation strategies proposed in this work are based on an explicit approach. The error estimate is computed injecting an enhanced approximation of the adjoint solution into the residual of the direct problem. The enhancement is based on a local postprocess of the computed eigenvectors, performed only once and not at each time step. This approach is very efficient for some quantities of interest in which the adjoint solution is fairly represented in a modal description.

The numerical examples show that the proposed estimates have a good effectivity for both the scalar and timeline quantities of interest, accounting both for space and time discretization errors. Contrary to other error estimates for linear visco-elastodynamics, the proposed estimates do not degenerate in the limit case of pure elasticity (i.e. when no damping is introduced in the formulation).

In current ongoing work, the proposed error estimation techniques are used as driving indicators for mesh adaptivity.

Acknowledgement

Partially supported by Ministerio de Educación y Ciencia, Grant DPI2011-27778-C02-02 and Universitat Politècnica de Catalunya (UPC-BarcelonaTech), grant UPC-FPU. The support of the Col·legi d'Enginyers de Camins, Canals i Ports (Catalunya) is also greatfuly acknowledged.

References

[1] Ainsworth M, Oden J. *A posteriori error estimation in Finite element analysis*. John Wiley & Sons Ltd., 2000.

[2] Ladevèze P, Pelle J. *La maîtrise du calcul en mécanique linéaire et non linéaire*. Lavoisier, 2001.

[3] Stein E. *Error–controlled adaptive finite elements in solid mechanics*. John Wiley & Sons Ltd., 2003.

[4] Ainsworth M, Oden J. A posteriori error estimation in finite element analysis. *Comput. Methods Appl. Mech. Engrg.* 1997; **142**:1–88.

[5] Gratsch T, Bathe K. A posteriori error estimation techniques in practical finite element analysis. *Computers and Structures* 2005; **83**:235–265.

[6] Babuŝka I, Rheinboldt W. Error estimates for adaptive finite element computations. *SIAM J. Numer. Anal.* 1978; **18**:736–754.

[7] Ladevèze P, Leguillon D. Error estimate procedure in the finite element method. *SIAM J. on Numerical Analysis* 1983; **20**:485–509.

[8] Zienkiewicz O, Zhu J. A simple error estimator and adaptative procedure for practical engineering analysis. *Int. J. Numer. Meth. Engrg.* 1987; **24**:337–357.

[9] Paraschivoiu M, Peraire J, Patera A. A posteriori finite element bounds for linear-functional outputs of elliptic partial differential equations. *Comput. Methods Appl. Mech. Engrg.* 1997; **150**:289–321.

[10] Parés N, Bonet J, Huerta A, Peraire J. The computation of bounds for linear-functional outputs of weak solutions to the two-dimensional elasicity equations. *Comput. Methods Appl. Mech. Engrg.* 2006; **195**:406–429.

[11] Cirak F, Ramm E. A posteriori error estimation and adaptivity for linear elasticity using the reciprocal theorem. *Comput. Methods Appl. Mech. Engrg.* 1998; **156**:351–362.

[12] Prudhomme S, Oden J. On goal–oriented error estimation for elliptic problems: application to the control of pointwise errors. *Comput. Methods Appl. Mech. Engrg.* 1999; **176**:313–331.

[13] Gallimard L, Ladeveze P, Pelle J. An enhanced error estimator on the constitutive relation for plasticity problems. *Computers and Structures* 2000; **78**:801–810.

[14] Ladevèze P. Constitutive relation errors for fe analysis considering (visco-)plasticity and damage. *Int. J. Numer. Meth. Engrg.* 2001; **52**:527–542.

[15] Ladevèze P, Moës N. Adaptive control for finite element analysis in plasticity. *Computers and Structures* 1999; **73**:45–60.

[16] Ladevèze P, Moës N, Douchin B. Constitutive relation error estimators for (visco)plastic finite element analysis with softening. *Comput. Methods Appl. Mech. Engrg.* 2000; **176**:247–264.

[17] Pares N, Diez P, Huerta A. Exact bounds of the advection-diffusion-reaction equation using flux-free error estimates. *SIAM J. Sci. Comput.* 2009; **31**:3064–3089.

[18] Larsson F, Diez P, Huerta A. A flux-free a posteriori error estimator for the incompressible Stokes problem using a mixed FE formulation. *Comput. Methods Appl. Mech. Engrg.* 2010; **199**:2383–2402.

[19] Parés N, Díez P, Huerta A. Bounds of functional outputs for parabolic problems. Part I: Exact bounds of the discontinuous galerkin time discretization. *Comput. Methods Appl. Mech. Engrg.* 2008; **197**:1641–1660.

[20] Parés N, Díez P, Huerta A. Bounds of functional outputs for parabolic problems. Part II: Bounds of the exact solution. *Comput. Methods Appl. Mech. Engrg.* 2008; **197**:1661–1679.

[21] Díez P, Calderon J. Goal-oriented error estimation for transient parabolic problems. *Comput. Mech.* 2007; **39**:631–646.

[22] Larson M, Bengzon F. Adaptive finite element approximation of multiphysics problems. *Commun. Numer. Methods Engrg.* 2008; **24**:505–521.

[23] Larson M, Soderlund R, Bengzon F. Adaptive finite element approximation of coupled flow and transport problems with applications in heat transfer. *Int. J. Numer. Meth. Fluids* 2008; **57**:1397–1420.

[24] Fick P, van Brummelen E, van der Zee K. On the adjoint-consistent formulation of interface conditions in goal-oriented error estimation and adaptivity for fluid-structure interaction. *Comput. Methods Appl. Mech. Engrg.* 2010; **199**:3369–3385.

[25] van der Zee K, van Brummelen E, Akkerman I, de Borst R. Goal-oriented error estimation and adaptivity for fluid-structure interaction using exact linearized adjoints. *Comput. Methods Appl. Mech. Engrg.* 2011; **200**:2738–2757.

[26] Asner L, Tavener S, Kay D. Adjoint-based a posteriori error estimation for coupled time-dependent systems. *SIAM J. Sci. Comput.* 2012; **34**:2394–2419.

[27] Li X, Wiberg N. Implementation and adaptivity of a space-time finite element method for structural dynamics. *Comput. Methods Appl. Mech. Engrg.* 1998; **156**:211–229.

[28] Wiberg N, Li X. Adaptive finite element procedures for linear and non-linear dynamics. *Int. J. Numer. Meth. Engrg.* 1999; **46**:178–1802.

[29] Schleupen A, Ramm E. Local and global error estimations in linear structural dynamics. *Computers and structures* 2000; **76**:741–756.

[30] Thompson L, He D. Adaptive space-time finite element methods for the wave equation on unbounded domains. *Comput. Methods Appl. Mech. Engrg.* 2005; **194**:1947–2000.

[31] Lahiri S, Bonet J, Peraire J. A variationally consistent mesh adaptation method for triangular elements in explicit lagrangian dynamics. *Int. J. Numer. Meth. Engng.* 2010; **82**:1073–1113.

[32] Aubry D, Lucas D, Tie B. Adaptive strategy for transient/coupled problems. Applications to thermoelasticity and elastodynamics. *Comput. Methods Appl. Mech. Engrg.* 1999; **176**:41–50.

[33] Bangerth W, Geiger M, Rannacher R. Adaptive Galerkin finite element methods for the wave equation. *Computational Methods in Applied Mathematics* 2010; **1**:3–48.

[34] Bangerth W. Adaptive Finite–Elemente–Methoden zur Lösung der Wellengleichung mit Anwendung in der Phisik der Sonne. PhD Thesis, Ruprecht–Karls–Universität Heidelberg 1998.

[35] Rannacher R. Adaptive Galerkin finite element methods for partil differential equations. *Journal of Computational and Applied Mathematics* 2001; **128**:205–233.

[36] Bangerth W, Rannacher R. Finite element approximation of the acoustic wave equation: error control and mesh adaptation. *East–West Journal of Numerical Mathematics* 1999; **7**:263–282.

[37] Bangerth W, Rannacher R. Adaptive finite element techniques for the acoustic wave equation. *Journal of Computational Acoustics* 2001; **9**:575–591.

[38] Combe J, Ladevèze P, Pelle J. Discretization error estimator for transcient dynamic simulations. *Advances in Engrg. Software* 2002; **33**:553–563.

[39] Combe J, Ladevèze P, Pelle J. Constitutive relation error estimator for transient finite element analysis. *Comput. Methods Appl. Mech. Engrg.* 1999; **176**:165–185.

[40] Ladevèze P, Pelle J. Estimation of discretization errors in dynamics. *Computers and Structures* 2003; **81**:1133–1148.

[41] Ladevèze P, Waeytens J. Model verification in dynamics trough strict upper bounds. *Comput. Methods Appl. Mech. Engrg.* 2009; **198**:1775–1784.

[42] Waeytens J. Contrôle des calculs en dynamique: bornes strictes et pertinents sur une quantié d'intérêt. PhD Thesis, LMT-Cachan 2010.

[43] Ladevèze P. Strict upper error bounds for computed outputs of interest in computational structural mechanics. *Computational Mechanics* 2008; **42**:271–286.

[44] Waeytens J, Chamoin L, Ladevèze P. Guaranteed error bounds on pointwise quantities of interest for transient viscodynamics problems. *Computational Mechanics* 2012; **49**:291–307.

[45] Verdugo F, Diez P. Computable bounds of functional outputs in linear visco-elastodynamics. *Comput. Methods Appl. Mech. Engrg.* 2012; **245–246**:313–330.

[46] Fuentes D, Littlefield D, Oden J, Prudhomme S. Extensions of goal-oriented error estimation methods to simulation of highly-nonlinear response of shock-loaded elastomer-reinforced structures. *Comput. Methods Appl. Mech. Engrg.* 2006; **195**:4659–4680.

[47] Carey V, Estep D, Johansson A, Larson M, Tavener S. Blockwise adaptivity for time dependent problems based on coarse scale adjoint solutions. *SIAM J. Sci. Comput.* 2010; **32**:2121–2145.

[48] Braack M, Burman E, Taschenberger N. Duality based a posteriori error estimation for quasi-periodic solutions using time averages. *SIAM J. Sci. Comput.* 2011; **33**:2199–2216.

[49] Wiberg N, Bausys R, Hager P. Adaptive h-version eigenfrequency analysis. *Computers and structures* 1999; **71**:565–584.

[50] Evans L. *Partial Differential Equations.* American Mathematical Society, 1998.

[51] Hughes J, Hulbert M. Space-time finite element methods for elastodynamics: Formulations and error estimates. *Comput. Methods Appl. Mech. Engrg.* 1988; **66**:339–363.

[52] Hulbert M, Hughes J. Space-time finite element methods for second-order hypeerbolic equations. *Comput. Methods Appl. Mech. Engrg.* 1990; **84**:327–348.

[53] Newmark N. A method of computation for structural dynamics. *J. of Engineering Mechanics* 1959; **85**:67–94.

[54] Bathe K. *Finite Element Procedures*. Prentice Hall, 1996.

[55] Rafique A, Kapre N, Constantinides G. A high throughput FPGA-based implementation of the lanczos method for the symmetric extremal eigenvalue problem. *8th International Symposium on Applied Reconfigurable Computing*, 2012.

[56] L–NTrefethen, Bau D. *Numerical linear algebra*. Society for Industrial & Applied Mathematics, 1997.

[57] Zienkiewicz O, Zhu J. The superconvergent patch recovery and a posteriori error estimates. part 1: The recovery technique. *Int. J. Numer. Meth. Engrg.* 1992; **33**:1331–1364.

[58] Wiberg N, Abdulwahab F, Li X. Error estimation and adaptive procedures based on superconvergent patch recovery. *Archives of Comput. Meth. in Engrg.* 1997; **4**:203–242.

[59] Díez P, Calderon J. Remeshing criteria and proper error representations for goal oriented h-adaptivity. *Comput. Methods Appl. Mech. Engrg.* 2007; **196**:719–733.

[60] Eriksson K, Johnson C, Logg A. Adaptive computational methods for parabolic problems. *Encyclopedia of Computational Mechanics*, vol. 1, Stein E, de Borst R, Hughes T (eds.). chap. 24, John Wiley, 2004.